Response Simulation of Reinforced Concrete Columns Under Lateral Loads

Mostafaei, H.; Hum, J. K.

Publisher's version / Version de l'éditeur:
https://doi.org/10.4224/20375047
Research Report (National Research Council of Canada. Institute for Research in Construction), 2010-02-01

Response Simulation of Reinforced Concrete Columns Under Lateral Loads

IRC-RR-294

Mostafaei, H.; Hum, J.K.

February 2010

NRC-CNRC

Response Simulation of Reinforced Concrete Columns under Lateral Loads

By H. Mostafaei, and J.K. Hum

Research Report RR-No.294

Date of Issue:

Abstract

A displacement-based evaluation approach is presented based on interactions of axial, shear, and flexure mechanisms to estimate lateral deformation and load capacities of typical reinforced concrete columns. The developed model is based on a modification and simplification of a relatively more complex approach known as the axial-shear-flexure interaction (ASFI) method, which is able to predict the full load-deformation response of reinforced concrete columns subjected to axial, flexure and shear forces. Two potential shear cracks are considered in the analysis: the primary shear crack, which is calculated in the strain field, and the secondary shear crack which is determined in the stress field. Plastic hinge length of the beam is defined and computed using the primary shear crack angle. Lateral load-deformation relations are obtained using this method for fifty-six typical rectangular reinforced concrete columns and the results were compared with the test data: consistent correlation and agreement were achieved. This paper describes the formulation, implementation and verification of the modified approach. A future attempt is to modify the ASFI method for response estimation of reinforced concrete columns in fire under axial load and lateral deformation induced by the thermal expansion.

Table of Contents

List of Tables

List of Figures

Notations

a_g	Maximum aggregate size
b	Width of the section
d	Effective depth of the section
d'	Cover concrete from the centre of the main compressive bars (first layer)
E_{sx}	Modulus of elasticity of the main reinforcement steel (in axial direction)
E_{sy}	Modulus of elasticity of the shear reinforcement steel (in transverse direction)
f_c'	Concrete compressive strength from the cylinder tests
f_{c1}	Concrete principal tensile stress in axial-shear model
f_{c2}	Concrete principal compression stress in axial-shear model
f_{ci}, f_{ci+1}	Concrete uniaxial compression stresses of the concrete stress blocks, at section i and i+1, in the axial-flexure model
f_{cx}	Concrete stress in x (axial) direction in axial-shear model
f_{cy}	Concrete stress in y (transverse) direction in axial-shear model
f_p	Concrete compressive strength (confinement effects included)
f_{sxy}	Yield stress of main reinforcement
f_{syy}	Yield stress of transverse reinforcement
h	Depth of the section
L_{in}	Length of the column from the inflection point to the end section
M	End-moment of the column
s_x	Average crack spacing in the axial direction, x-direction
s_y	Average crack spacing in the transverse direction, y-direction
s_θ	Average crack spacing, perpendicular to the cracks
V_u	Total shear force of the column
w	Shear crack width
x	Distance from the inflection point of the column to an arbitrary section along the column
β	compression softening factor
δ	Total lateral drift/deformation of column
ε_1	Concrete principal tensile strain in axial-shear model
ε_2	Concrete principal compression strain in axial-shear model
ε_c'	Concrete peak compressive strain
ε_{cf}	Centroidal strain of the flexure section in the axial-flexure model

ε_{ci}, ε_{ci+1} Concrete uniaxial compression strains corresponding to the resultant forces of the concrete stress blocks, at section i and i+1, in the axial-flexure model

ε_{cs} Axial/centroidal strain in axial-shear model

ε_{p} Concrete peak compressive strain (effects of confinement included)

ε_{x} Total axial strain (in x direction)

ε_{xa} Total pure axial strain due to only the applied axial load

ε_{xaf} Pure axial strain due to only the applied axial load in axial-flexure model

ε_{xas} Pure axial strain due to only the applied axial load in axial-shear model

ε_{xf} Flexural-axial strain due to the flexure deformation/crack

ε_{xs} Shear-axial strain due to the shear deformation/crack

ε_{y} Total transverse strain

γ Total lateral drift ratio

γ_{f} Flexural drift ratio in axial-flexure model

γ_{s} Shear strain/ drift ratio in axial-shear model

θ_{c} Primary shear crack angle

θ_{cc} Secondary shear crack angle

ρ_{sy} Shear reinforcement ratio in y (transverse) direction

ρ_{sx} Main reinforcement ratio in x direction

σ_{x} Total applied axial stress

σ_{xf} Axial stress in axial-flexure model

σ_{xs} Axial stress in axial-shear model

σ_{y} Total normal stress in y direction, perpendicular to the longitudinal axis of the column

σ_{z} Total normal stress in z direction, perpendicular to the longitudinal axis of the column

τ Total shear stress

τ_{f} Shear stress in axial-flexure model

τ_{i} shear stress transferred by aggregate interlock across the crack surface

τ_{s} Shear stress in axial-shear model

ϕ Curvature at the flexure section (in axial-flexure model) varied along the column

Introduction

Evaluation and estimation of ductility and ultimate lateral deformation capacity of reinforced concrete columns have always been challenging for design engineers and researchers. Design of reinforced concrete columns under lateral loads requires a minimum ductility for the elements. The more ductile a column is designed, the higher lateral deformation is sustained by the column. The lateral deformations are the results of the applied lateral loads such as earthquake, winds, and the floor thermal expansion in fire. Figure 1 shows an example of the column's lateral deformations in fire due to the thermal expansion. Figure 1a illustrates shear failure of a column on the 6th floor of the US Military Personnel Records Centre building due to the fire that occurred in 1973 (Bailey 2004), and Figure 1b demonstrates how the thermal expansion induces lateral deformation to the columns.

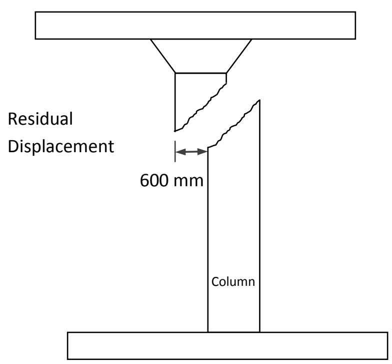

Figure 1a) Shear failure of a column in fire, Military Personnel Records Centre building in the USA

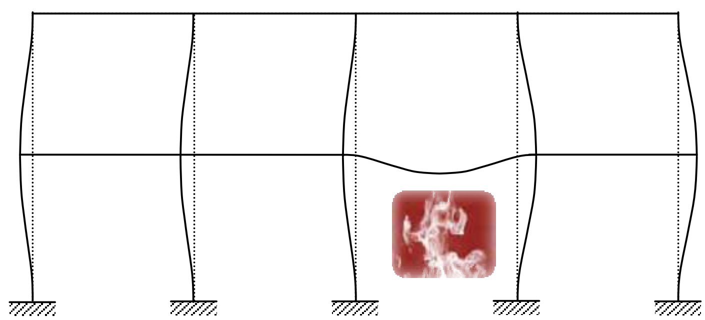

Figure 1b) A building frame exposed to fire

Figure 1. Lateral deformation of columns in fire due to the structural thermal expansions.

Although the response of reinforced concrete columns under lateral loads has been studied for many years, a remaining challenge has been the development of a reliable methodology for estimating the ultimate deformation capacity of columns. In fire, studies are limited to columns under axial loads only. There is a lack of research on performance columns in fire under lateral deformation. This report explores the lateral deformation response of columns at ambient temperature. A future extension of this study is to include the effect of fire on the lateral column response.

Studies by different researchers, such as Elwood and Moehle (2005), Park et al. (1982),.Lynn et al. (1996), show that lateral deformation capacity of the columns are significantly dependent not only on their axial and moment capacity but mostly on their shear capacity. Mostafaei and Kabeyasawa (2007) developed a displacement-based analytical method for modeling the load-deformation response of reinforced concrete columns under axial and lateral loads. The model was developed to include the effects of shear deformations in sectional analyses through a method called Axial-Shear-Flexure Interaction (ASFI). The main deformation component of the interaction was the axial deformation, which was extracted from an axial-flexure model and manipulated into an axial-shear model. In this method, the flexure mechanism was modeled by applying traditional section analysis techniques, and the shear behavior was modeled based on the Modified Compression Field Theory (MCFT), (Vecchio and Collins 1986). One of the assumptions of the ASFI method was that when the compression stress of the cover concrete, at the post peak, drops to about 30% of its compression strength, it reaches an ultimate deformation capacity state. The study suggested further investigation on this and simplification of the method for use in practice.

Later, the shear model of the ASFI method was simplified and a method called the Uniaxial-Shear-Flexure Model (USFM) was developed (Mostafaei and Vecchio 2008). Unlike the original ASFI method where fiber elements were used to model the column's section, in the USFM method, only one compression stress block was employed to simulate the cross section concrete stress distribution. In both the ASFI and the USFM methods a compression softening factor was applied to the concrete element in compression which was determined according to the tensile strain of the concrete of the shear element. Later, further simplifications were made in the USFM models by defining three general failure criteria for reinforced concrete columns (Mostafaei et al. 2009-a). The three main failures, for typical reinforced concrete columns in buildings, are tension-shear failure across cracks, loss of concrete compression strength, and compression-shear failure, for both shear- and flexure-dominated members. In this method, for simplicity, the compression softening factor was not applied in the section analysis. However, the method had some limitations for columns with very low applied shear stress. This is the condition at which most of the shear deformation occurs in the plastic hinge. Later, Mostafaei et al. (2009-b) modified the approach to include a plastic hinge length and the distribution of the shear strain along the column. This was needed to improve the deformation response of the columns with very low applied shear stress.

This report presents the latest modifications of the ASFI and the USFM methods. These include estimation of the shear cracks in both stress and strain fields. For simplicity, no compression softening factor is employed in the section analysis. The tensile strain of concrete is determined according to the shear strain, concrete strain in x direction and the principal compression stress. This will eliminate the iterations used in the previous USFM method for the tensile stress of concrete of the shear element. One of the main assumptions in this method is that strain in the transverse bars yields at the ultimate stage.

A future modification is to employ the ASFI method for response prediction of reinforced concrete columns in fire and after fire exposure. This includes post-fire seismic capacity and thermal lateral deformation capacity of the reinforced concrete columns.

Methodology of the Axial-Shear-Shear-Flexure Interaction

The main concept and methodology of the axial-shear-flexure interaction (ASFI) method are based on the axial deformation interaction between the two models: a flexure model based on traditional uniaxial section analysis principles, and a shear model based on a biaxial shear element approach.

Figure 2 illustrates the interactions between shear and flexure deformations/cracks. The figure shows how the flexure deformation results in an increase in the centroidal strain, which in turn enlarges the shear crack and deformation. The centroidal strain in the flexure mechanism, ε_{cf}, of the axial-flexure model, is composed of the pure axial strain, ε_{xaf}, due to only the applied axial load, and flexural-axial strain, ε_{xf}, due to the flexure deformation/crack. On the other hand, centroidal strain in shear mechanism, ε_{cs}, of the axial-shear model, is composed of the pure axial strain, ε_{xas}, due to only the applied axial load, and shear-axial strain, ε_{xs}, due to the shear deformation/crack. The compatibility condition requires identical axial deformation due to the applied axial load for the two mechanisms; thus, $\varepsilon_{xa} = \varepsilon_{xaf} = \varepsilon_{xas}$. Therefore, the total column's axial deformation, ε_x, is defined as.

$$\varepsilon_x = \varepsilon_{xa} + \varepsilon_{xs} + \varepsilon_{xf} \tag{1}$$

To obtain ε_x in Eq. (1), ε_{xf} must be extracted from ε_{cf} and added to ε_{cs}. The total lateral drift of a column, γ, is defined as the sum of shear strain, γ_s, and the flexural drift ratio, γ_f, between the two sections.

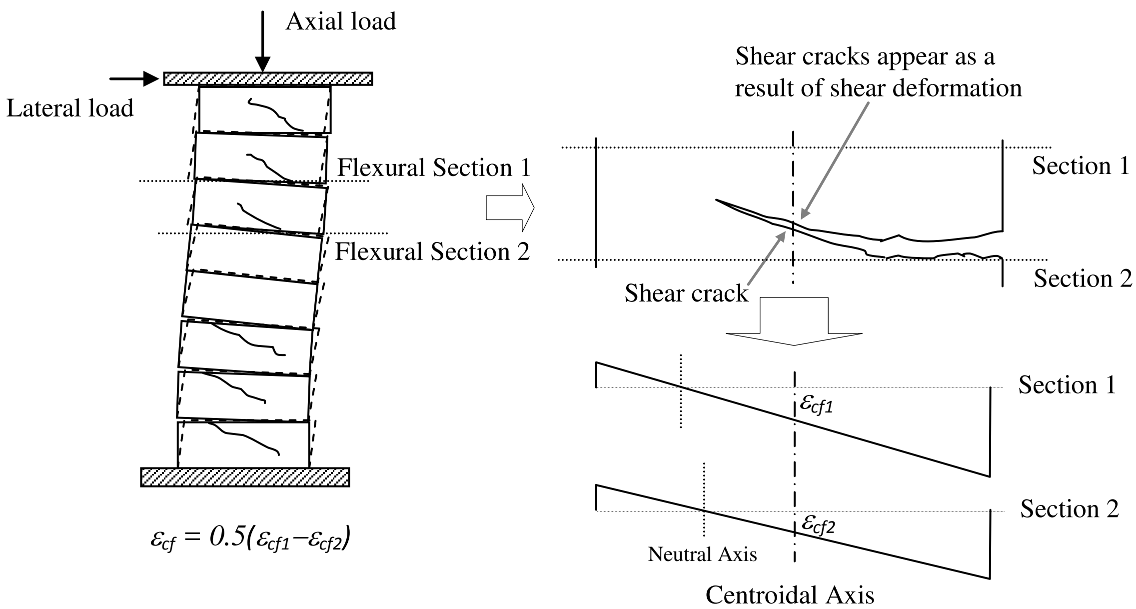

Figure 2. Effect of flexural deformation on shear crack widening in a reinforced concrete column.

$$\gamma = \gamma_s + \gamma_f \tag{2}$$

The pullout effect is ignored in this study. Equilibrium of the shear and axial stresses from the axial-flexure model, τ_f and σ_{xf}, and from the axial-shear model, τ_s and σ_{xs}, respectively, must be satisfied simultaneously through the analysis. That is,

$$\sigma_{xf} = \sigma_{xs} = \sigma_x \tag{3}$$

$$\tau_f = \tau_s = \tau \tag{4}$$

where σ_{xf} = axial stress in the axial-flexure mechanism; σ_{xs} = axial stress in the axial-shear mechanism; σ_x = applied axial stress; τ_f = shear stress in the axial-flexure mechanism; τ_s = shear stress in the axial-shear mechanism, and τ = applied shear stress. Stresses in axes perpendicular to the longitudinal axis of the column (i.e., the clamping stresses σ_y and σ_z) are ignored by assuming equilibrium between the confinement pressure and the hoops stresses.

$$\sigma_y = \sigma_z = 0 \tag{5}$$

Figure 3 illustrates the ASFI method for a reinforced concrete column with two end sections, including the equilibrium and compatibility conditions.

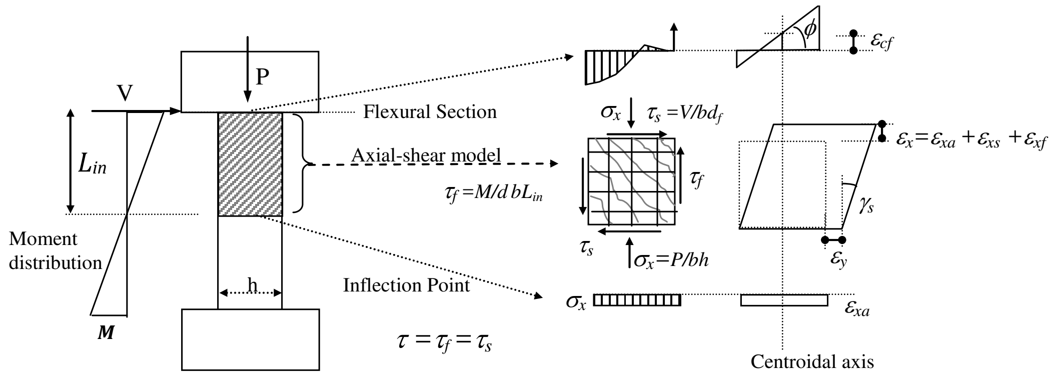

Figure 3. Axial-shear-flexure interactions in ASFI method.

The same assumption as that in the USFM is made here for the average concrete compression strain. Figure 4 shows a reinforced concrete column of moderate height, fixed against rotation and translation at the bottom and free at the top, subjected to in-plane lateral load and axial load. Given its pattern along the column (see Figure 4-a), the concrete principal compression strain for a shear element between the two sections, ε_2, may be determined based on average values of the concrete uniaxial compression strains corresponding to the resultant forces of the concrete stress blocks.

$$\varepsilon_2 = 0.5(\varepsilon_{ci} + \varepsilon_{ci+1}) \tag{6}$$

For the column in Figure 4, the compression strain obtained from the above equation is set equal to the average principal compression strain of the element between the two sections *i* and *i*+1.

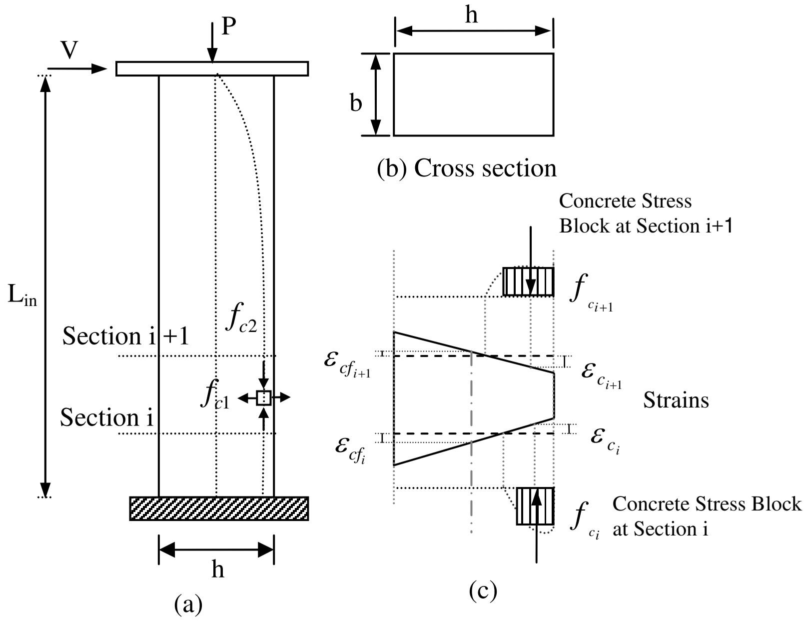

Figure 4. A reinforced concrete column subjected to shear and axial loads; a) Concrete principal compression stress pattern, b) Cross section, and c) Stress blocks and strains at two adjacent sections.

The shear mechanism is modeled according to the Modified Compression Field Theory (MCFT), (Vecchio and Collins 1986).

Ultimate States and Failures

There are three ultimate states defined for a reinforced concrete column under axial and shear load: shear failure at the crack (Mode 1 Failure); failure due to loss of compression strength (Mode 2 Failure), and shear-compression failure (Mode 3 Failure). Mode 3 could result in lateral load degradation. However, larger lateral deformation capacity can be observed mainly for ductile columns.

The three failure modes are described for a typical column, such as the one shown in Fig. 3, with a flexure section at one end, a section at the inflection point and a shear model between the two sections.

- Mode 1 - Shear failure at the crack

This is a failure that occurs at the shear crack due to loss of concrete shear strength at the crack. Mode 1 failure, which is typically the governing case for columns with low transverse reinforcement ratios, occurs when (Mostafaei et al. 2009-a):

$$\tau_f = \frac{M}{bdL_{in}} \geq \tau_i + f_{syy}\rho_{sy}\cot\theta_c \tag{7}$$

where τ_f is shear stress due to flexure mechanism; *M* is the end-moment of the column; *d* is the effective depth of the section, *b* is the width of the section; L_{in} is the length of the column from the inflection point to the end section; θ_c is the crack angle, f_{syy} is the yield stress of transverse reinforcement, ρ_{sy} is the reinforcement ratio in the y (transverse) direction, and τ_i is the shear stress transferred by aggregate interlock across the crack surface, determined by Walraven's equation, Eq. (8).

$$\tau_i \leq \frac{0.18\sqrt{f_c'}}{0.31 + \dfrac{24w}{a_g + 16}} \ \text{(MPa, mm)} \tag{8}$$

with $w = s_\theta \varepsilon_1$, and $s_\theta = \dfrac{1}{\dfrac{\sin\theta_c}{s_x} + \dfrac{\cos\theta_c}{s_y}}$,

where f_c' is the concrete compressive strength; *w* is the average crack width; ε_1 is the concrete tensile strain in shear element; s_x and s_y are the average crack spacings in the x- and y-directions, respectively, and a_g; is the maximum aggregate size. In this study, s_x and s_y are the same as the maximum reinforcement spacing in the x- and y-directions, respectively.

- Mode 2 - Loss of compression strength

Columns under high shear force, such as short columns, if not failing via Mode 1, may lose compression strength, f_2, due to shear deformation, which results in loss of shear strength. Mode 2, takes place when (Mostafaei et al. 2009-a):

$$\tau_f = \frac{M}{bdL_{in}} \geq \frac{(f_{c1} - f_{c2})}{(\tan\theta_c + 1/\tan\theta_c)} \tag{9}$$

where f_{c1} and f_{c2} are the tensile stress and compression stress in the concrete according to the shear model.

- *Mode 3 - Concrete post-peak state*

Although Mode 3 is considered a failure mode, since concrete is at the post peak, columns with high lateral reinforcement likely sustain larger lateral deformation not with a significant load reduction. In this case, the columns normally fail in Modes 1 or 2 after experiencing Mode 3. The level of lateral deformation capacity is dependent on the level of the column's confinement and the level of the damage caused to the confinement as the result of a cycling loading.

Mode 3 occurs when $\varepsilon_2 = \varepsilon_c'$.

In this approach, the concrete compression softening factor was employed only within the MCFT-based shear model. This is because at the compression block of the flexure section, crack angle is nearly zero.

Shear Cracks

For this study, two shear cracks are considered in the analysis: primary shear crack, θ_c, and the secondary shear crack, θ_{cc}. The failure modes described in the previous section must be checked for both of these two cracks.

- *Primary shear crack*, θ_c,

This is the shear crack of the shear model which is calculated in the strain field.

$$\tan^2 \theta_c = \frac{\varepsilon_x - \varepsilon_2}{\varepsilon_y - \varepsilon_2} \tag{10}$$

It is assumed that strain of lateral reinforcement, ε_y, is at the yield strain. In other words, when the hoops' strain reaches yielding of the bars, the failure occurs. This assumption was made based on the observation in experimental studies (Ousalem et al. 2003). This assumption eases the analysis by avoiding the iteration process.

- *Secondary shear crack*, θ_c,

The secondary shear crack is determined in the stress filed using the following equation:

$$\tan\theta_{cc} = \sqrt{\frac{(f_{c1} - f_{cy})}{(f_{c1} - f_{cx})}} \tag{11}$$

where $f_{cy} = -\rho_{sy} f_{syy}$ (Since hoops are considered yielded); $f_{cx} = \sigma_x - \rho_{sx} E_{sx} \varepsilon_x$; E_{sx} is the modulus of elasticity of the main reinforcement steel; ρ_{sx} is the reinforcement ratio in the x-direction (main bars), and tensile concrete stress is $f_{c1} = \frac{0.33\sqrt{f_c'}}{1+\sqrt{500\varepsilon_1}}$ (Vecchio and Collins 1986), where ε_1 is the tensile strain of concrete, determined from the principal strains relation.

$$\varepsilon_1 = \frac{(\frac{\gamma_s}{2})^2}{(\varepsilon_x - \varepsilon_2)} + \varepsilon_x \tag{12}$$

The secondary shear crack becomes almost constant when both longitudinal and transverse bars yield. However, it changes when average axial deformation of the column reduces to zero or even a negative value, which results in a compression failure.

In general, the primary shear crack represents the crack at the plastic zones, and the secondary crack represents the overall response of the column at the inflection point.

Analytical Steps

Using the described approach, an analytical procedure is constructed to estimate the ultimate deformation of a reinforced concrete column subjected to both axial and lateral loads.

The step-by-step calculation using the new method is provided here for a column specimen (Specimen CB060C) tested by Amitsu et al. 1991 at the pre-peak state.

1. Assume an initial value for the concrete compression strain of the flexure section. ε_c; for example, $\varepsilon_c = -0.002618$

2. Employ a section analysis for the end section of the column and determine the centroidal strain of the section, ε_{cf}, in Fig. 3 (Mostafaei et al. 2009).

$\varepsilon_{cf} = -0.001502$

3. Determine the axial strain at the inflection point with zero moment, ε_{xa}, in Fig. 3. This is the axial deformation of the column when it is subjected only to axial load.

$\varepsilon_{xa} = -0.00062$

4. Compute the average concrete principal compression strain, ε_2, and average axial strain, ε_x, for the shear model.

$$\varepsilon_2 = \frac{\varepsilon_c + \varepsilon_{xa}}{2} \tag{13}$$

$$\varepsilon_2 = \frac{\varepsilon_c + \varepsilon_{xa}}{2} = -0.00162$$

$$\varepsilon_x = \frac{\varepsilon_{cf} + \varepsilon_{xa}}{2} \tag{14}$$

$$\varepsilon_x = \frac{\varepsilon_{cf} + \varepsilon_{xa}}{2} = -0.00106$$

5. It is considered that at the ultimate failure stage, hoops are yielded, therefore:

$\varepsilon_y = 0.002$

6. Determine $\tan\theta_c$

$$\tan\theta_c = \sqrt{\frac{\varepsilon_x - \varepsilon_2}{\varepsilon_y - \varepsilon_2}} = 0.39$$

7. Determine shear strain:

7.1. Maximum shear strain:

$$\gamma_s = \frac{2(\varepsilon_x - \varepsilon_2)}{\tan\theta_c} \tag{15}$$

$$\gamma_s = \frac{2(\varepsilon_x - \varepsilon_2)}{\tan\theta_c} = 0.0028$$

7.2. Average shear strain for the entire column

$$\gamma_{s-ave} = \frac{(2h/\tan\theta)}{L}\gamma_s \le \gamma_s \qquad (16)$$

$$\gamma_{s-ave} = \frac{\min(2\times 278/0.39)}{646}0.0028 = 0.006 > \gamma_s$$

Therefore, $\gamma_{s-ave} = \gamma_s = 0.0028$

8. Determine the tensile strain:

$$\varepsilon_1 = \frac{(\frac{\gamma_s}{2})^2}{(\varepsilon_x - \varepsilon_2)} + \varepsilon_x = \frac{(\frac{0.0028}{2})^2}{(-0.00106 + 0.00162_2)} - 0.00106 = 0.0025$$

Note: shear deformation, γ_s, is determined based on the primary shear crack angle.

9. Determine the secondary crack angle:

$$\tan\theta_{cc} = \sqrt{\frac{(f_{c1} - f_{cy})}{(f_{c1} - f_{cx})}} = \sqrt{\frac{(1.06 - (-3.23))}{(1.06 - (-25.29))}} = 0.404$$

where $f_{c1} = \frac{0.33\sqrt{f'_c}}{1+\sqrt{500\varepsilon_1}}\frac{0.33\sqrt{46.3}}{1+\sqrt{500(0.0025)}} = 1.06MPa$

10. Calculate compression softening factor and concrete compression stress:

$$\beta = \frac{1}{0.8 - 0.34\frac{\varepsilon_1}{\varepsilon'_c}} \qquad (17)$$

$$\beta = \frac{1}{0.8 - 0.34\frac{\varepsilon_1}{\varepsilon'_c}} = \frac{1}{0.8 - 0.34\frac{0.0025}{-0.002}} = 0.81$$

Based on the strain stress relation of concrete

$$f_{c2} = \beta f_p (\frac{2\varepsilon_2}{\varepsilon_p} - (\frac{\varepsilon_2}{\varepsilon_p})^2) \tag{18}$$

$$f_{c2} = 0.81 \times 50.9(\frac{2(-0.0016)}{-0.0022} - (\frac{-0.0016}{-0.0022})^2) = 38MPa$$

12. Check for failure employing the two shear crack angles of θ_c and θ_{cc}.

- *Check for Mode 1 – Shear failure at the crack*

$$\tau_i \leq \frac{0.18\sqrt{f_c'}}{0.31 + \frac{24w}{a_g + 16}} = \frac{0.18\sqrt{46.3}}{0.31 + \frac{24(0.11)}{10 + 16}} = 2.99MPa$$

where the maximum aggregate size is assumed as *a_g=10mm*; the crack spacing S_θ=42 mm, and therefore, the crack width is $w = \varepsilon_1 S_\theta = 0.0025 \times 42 = 0.11mm$

Hence:

$$\tau_f = \frac{M}{bdL_{in}} = \frac{1.72 \times 10^8}{(278)(250)(646/2)} = 7.66MPa$$

$$\tau_f = \frac{M}{bdL_{in}} = 7.66MPa < \tau_i + f_{syy}\rho_{sy}\cot\theta_c = 2.99 + 0.0078 \times 414(1/(0.39)) = 11.2MPa$$

$$\tau_f = \frac{M}{bdL_{in}} = 7.66MPa < \tau_i + f_{syy}\rho_{sy}\cot\theta_{cc} = 2.99 + 0.0078 \times 414(1/(0.404)) = 11.0MPa$$

Both above conditions are fine. Mode 1 is not a failure mode for this specimen until this stage.

- *Check for Mode 2 – Loss of compression strength*

This failure mode also needs to be checked at both shear cracks:

$$\tau_f = \frac{M}{bdL_{in}} = 7.66MPa < \frac{(f_{c1} - f_{c2})}{(\tan\theta_c + 1/\tan\theta_c)} = \frac{(1.06-(-38))}{(0.39+1/0.39)} = 13.2MPa$$

$$\tau_f = \frac{M}{bdL_{in}} = 7.66MPa < \frac{(f_{c1} - f_{c2})}{(\tan\theta_{cc} + 1/\tan\theta_{cc})} = \frac{(1.06-(-38))}{(0.404+1/0.404)} = 13..6MPa$$

Therefore, Mode 2 of failure did not occur.

- Mode 3 – Concrete post-peak state

Since $\varepsilon_2 = -0.0016 > \varepsilon'_c = -0.002$,Mode 3 also is not a failure mode. For columns with failure Mode 3, the analysis can be continued until one of the other two failure modes occur or the lateral load drops significantly (for instance to 70% of the maximum load).

13. Determine the ultimate lateral deformation using Eq. (2), when:

Flexural lateral deformation is calculated using the same approach employed in the original ASFI method (Mostafaei, 2006), however, the plastic zone length is determined according to the primary shear crack angle and limited by the column's geometries.

$$\gamma_f = \frac{\delta}{L_{in}} = \frac{1}{L_{in}} \int_0^{Lin} x\phi dx\,, \tag{19}$$

Plastic hinge is determined based on the shear crack angle by:

$$L_p = h/(2\tan\theta_c) \leq (0.5L_{in} \quad and \quad 0.5h) \tag{20}$$

$$L_p = 278/(2(0.39)) \leq (0.5(646/2) \quad and \quad 0.5(278)) = 139mm$$

Hence, $\gamma_f = \frac{\delta}{L_{in}} = \frac{1}{L_{in}} \int_0^{Lin} x\phi dx = 0.0024$.

For the sake of comparison, lateral deformations are determined for the column for two cases:

- Lateral deformation due only to section analysis.

and $\gamma = \gamma_f = 0.0024$

- Lateral deformation due to both flexure and shear analysis

and $\gamma = \gamma_f + \gamma_s = 0.0024 + 0.0028 = 0.0052$

14. Finally, the ultimate lateral load capacity is obtained by

$$V_u = \tau_f bd[L_{in} /(L_{in} - d')] \tag{21}$$

$V_u = 7.66(278)(250)[323/(323-28)] = 582 \quad kN$

where h is the depth of the section, and d' is the cover concrete. Shear force in Eq. (21) has been increased for consideration of the support confinement effect. This is typically because column's specimens are built with relatively rigid supports which provide confinement to the columns at the plastic hinge zones. Such an effect is considered by determining an effective column length as: $(L_{in} - d')$. Further studies are required to define and determine the effective length considering the confinement effect. In this study, all the analysis were carried out according to the above effective length.

Furthermore, other possible failure modes such as buckling of the compression bars, bond failure, failure of the cover concrete, and rupture of tensile bars must be checked for the columns. In this study, these modes were not checked in the analysis of the column specimens

Model Verification

The analytical process described in this report was implemented for 55 typical reinforced concrete columns with normal strength concrete and square cross sections. The column specimens were selected from 17 individual test reports published by various authors in different countries around the world as listed in Table 1. A macro was created using Excel to carry out an analysis for all the column specimens in one run. Comparisons between the experimental data and analytical results are plotted in Figures 5 to 59 indicating a consistently acceptable fit for most of the cases. The results particularly show reasonable predictions for the ultimate deformation capacity of the columns.

Conclusions

The Uniaxial-Shear-Flexure Model, which is a simplified method of the Axial-Shear-Flexure Interaction Approach, was modified to include a secondary shear crack. The new analytical procedure does not require an iteration process for the shear model. Plastic hinge length is determined according to a shear crack angle at the zone. The most important factors in determining the lateral deformation capacity of the columns was the amount of transverse reinforcement, and most importantly, the column confinement factor. For simplicity, no compression softening was applied to the concrete compression block of the section analysis. However, such an assumption seems not to have significant effects on the columns response. Only one stress block is representing the compressive concrete in the section analysis. Should the model be implemented using a computer programming, a fiber model could be implemented for a better concrete stress distribution on the cross section. The failure modes defined for this method are checked during the analysis for two possible shear cracks: a primary shear crack which is determined in the strain field and a secondary shear crack which is obtained in the stress field. The ultimate deformation and load capacity results, obtained by the modified approach, were verified against experimental data, and a consistent fit between the analytical and experimental results, for a series of reinforced concrete columns, were obtained.

References

Amitsu, Shigeyuki; Shirai, Nobuaki; Adachi, Hiromi; and Ono, Arata (1991). "Deformation of Reinforced Concrete Column with High or Fluctuating Axial Force," Transactions *of the Japan Concrete Institute*, Vol. 13, pp. 355-362.

Arakawa, T., Arai, Y., Egashira, K., and Fujita, Y. (1982). "Effects of the Rate of Cyclic Loading on the Load-Carrying Capacity and Inelastic Behavior of Reinforced Concrete Columns," *Transactions of the Japan Concrete Institute*, Vol. 4.

Arakawa, T., Arai, Y., Mizoguchi, M., and Yoshida, M. (1989). "Shear Resisting Behavior of Short Reinforced Concrete Columns Under Biaxial Bending-Shear," *Transactions of the Japan Concrete Institute*, Vol. 11, 1989, pp. 317-324.

Azizinamini, A., Johal, L.S., Hanson, N.W., Musser, D.W., and Corley, W.G. (1988). "Effects of Transverse Reinforcement on Seismic Performance of Columns - A Partial Parametric Investigation," Project No. CR-9617, *Construction Technology Laboratories*, Research Report.

Bailey CG. (2004). “Membrane Action of Slab/Beam Composite Floor Systems in Fire.”, *Engineering Structures*, 16, 1691-1703.

Bett, B.J.; Klingner, R.E.; and Jirsa, J.O. (1985). "Behavior of Strengthened and Repaired Reinforced Concrete Columns Under Cyclic Deformations," PMFSEL Report No. 85-3 Department of Civil Engineering, *University of Texas at Austin*, Austin, Texas

Elwood, K.J. and Moehle J.P. (2005). "Drift Capacity of Reinforced Concrete Columns with Light Transverse Reinforcement." *Earthquake Spectra*, Earthquake Engineering Research Institute, 21, 71-89.

Ghee, A.B., Priestley, M.J.N., and Park, R. (1981). "Ductility of Reinforced Bridge Piers Under Seismic Loading," Report 81-3, Department of Civil Engineering, *University of Canterbury*, Christchurch, New Zealand, February, 109 pages.

Kono, S.; and Watanabe, F. (2000). “Damage Evaluation of Reinforced Concrete Columns under Multiaxial Cyclic Loadings.” *The Second U.S.-Japan Workshop on Performance-Based Earthquake Engineering Methodology for Reinforced Concrete Building Structures*, 221-231.

Kono, S., Arai, Y., Hakim, B., Watanabe, F. (2003). "Damage Assessment of Reinforced Concrete Columns Under High Axial Loading", ICPCM- A New Era of Building, Cairo, Egypt, 2003.

Lynn, A.C., Moehle, J.P., Mahin, S. A., and Holmes, W. T. (1996). “Seismic evaluation of existing reinforced concrete building columns.” *Earthquake Spectra*, 12(4), 715–739.

Matamoros, A.B. (1999). "Study of Drift Limits for High-Strength Concrete Columns," Department of Civil Engineering, *University of Illinois at Urbana-Champaign*, Urbana, Illinois.

Mo, Y.L.; and Wang, S.J. (2000). "Seismic Behavior of RC Columns with Various Tie Configurations", *Journal of Structural Engineering*, ASCE, Vol. 126 No.10, pp. 1122-1130

Mostafaei, H., (2006). “Axial-shear-flexure interaction approach for displacement-based evaluation of reinforced concrete elements.” *The University of Tokyo*, PhD Thesis.

Mostafaei, H., and Kabeyasawa, T. (2007). “Axial-Shear-Flexure Interaction Approach for Reinforced Concrete Columns.” *ACI Structural Journal*, 104(2), 218-226.

Mostafaei, H., and Vecchio, F. J. (2008). “Uniaxial Shear-Flexure Model for Reinforced Concrete Elements.” *ASCE Journal of Structural Engineering*, 134(9), 1538-1547.

Mostafaei, H., Vecchio, F.J., and Kabeyasawa T. (2009-a). “Deformation Capacity of Reinforced Concrete Columns.” *ACI Structural Journal*, 106(2), 187-195.

Mostafaei, H., Vecchio, F.J., and Kabeyasawa T. (2009-b).“A Simplified Axial-Shear-Flexure Interaction Approach for Load and Displacement Capacity of Reinforced Concrete Columns.” *The ATC-ASCE conference on Improving the Seismic Performance of Existing Buildings and Other Structures, ASCE*, San Francesco, December 9-11.

Ohno, T., and Nishioka, T. (1984). "An Experimental Study on Energy Absorption Capacity of Columns in Reinforced Concrete Structures," *Proceedings of the JSCE, Structural Engineering/Earthquake Engineering*, Vol. 1, No 2, pp. 137-147.

Ohue, M., Morimoto, H., Fujii, S., and Morita, S. (1985). "The Behavior of R.C. Short Columns Failing in Splitting Bond-Shear Under Dynamic Lateral Loading," *Transactions of the Japan Concrete Institute*, Vol. 7, pp. 293-300.

Ono, A., Shirai, N., Adachi, H., and Sakamaki, Y. (1989). "Elasto-Plastic Behavior of Reinforced Concrete Column With Fluctuating Axial Force," *Transactions of the Japan Concrete Institute*, Vol. 11, pp. 239-246.

Ousalem, H., Kabeyasawa, T., Tasai, A., Iwamoto, J. (2003). “Effect of Hysteretic Reversals on Lateral and Axial Capacities of Reinforced Concrete Columns.” *Proceedings of the Japan Concrete Institute*, 25 (2), pp.367-372.

Park, R., Priestley, M.J.N., Gill, W.D. (1982). “Ductility of square confined concrete columns.” *Journal of Structural Division ASCE*, 108(4), 929–950.

Saatcioglu, M., and Ozcebe, G. (1989). "Response of Reinforced Concrete Columns to Simulated Seismic Loading," American Concrete Institute, *ACI Structural Journal*, January - February, pp. 3-12.

Soesianawati, M.T.; Park, R; and Priestley, M.J.N. (1986). "Limited Ductility Design of Reinforced Concrete Columns," Report 86-10, Department of Civil Engineering, *University of Canterbury*, Christchurch, New Zealand, 208 pages.

Tanaka, H., and Park, R. (1990). "Effect of Lateral Confining Reinforcement on the Ductile Behavior of Reinforced Concrete Columns." *University of Canterbury*, Report 90-2, Department of Civil Engineering, pp. 458.

Vecchio, F.J., and Collins, M.P. (1986). “The Modified Compression Field Theory for Reinforced Concrete Elements Subjected to Shear.” *ACI Journal*, 83(2), 219-231.

Zahn, F.A.; Park, R; and Priestley, M.J.N. (1986). "Design of Reinforced Bridge Columns for Strength and Ductility," Report 86-7, Department of Civil Engineering, *University of Canterbury*, Christchurch, New Zealand, 330 pages.

Table 1. Material property of the test specimens.

Specimen	Type	b mm	h mm	$2L_{in}$ mm	S_h mm	ρ_g %	ρ_w %	f_{syx} MPa	f_{syy} MPa	f'_c MPa	P kN
CB060C[1]	DC	278	278	646	52	4.12	0.78	413.9	441.2	46.3	2632
No. 102[2]	DC	250	250	750	32	0.75	1.19	322.7	392.9	20.6	429
OA2[3]	DC	180	180	450	64	3.28	0.22	249.2	340.4	31.8	191
OA5[3]	DC	180	180	450	64	3.28	0.22	249.2	340.4	33.1	477
NC-2[4]	DE	457	457	2743	103	1.94	1.08	453.7	439.2	39.3	1690
NC-4[4]	DE	457	457	2743	103	1.94	0.61	616.4	439.2	39.9	2580
No. 1-1[5]	DC	305	305	914	203	2.45	0.18	413.7	461.9	29.9	288
1981, No. 3[6]	DE	400	400	3200	100	1.51	1.70	320.0	427.0	23.6	1435
1981, No. 4[6]	DE	400	400	3200	90	1.51	1.31	280.0	427.0	25.0	840
D1N3[7]	C	242	242	1250	40	2.72	0.78	486.0	461.0	37.6	661
D1N6[7]	C	242	242	1250	40	2.72	0.78	486.0	461.0	37.6	1321
L1D60[8]	C	600	600	2400	100	1.64	1.33	524.0	388.0	39.2	8000
L1N60[8]	C	600	600	2400	100	1.64	1.33	524.0	388.0	39.2	8000
L1D6B[8]	C	560	560	2400	100	1.88	1.42	524.0	388.0	32.2	6000
C5-00N[9]	C	203	203	1220	76	1.93	0.92	502.2	572.3	37.9	0
C5-00S[9]	C	203	203	1220	76	1.93	0.92	502.2	572.3	37.9	0
C5-20N[9]	C	203	203	1220	76	1.93	0.92	406.8	586.1	48.3	285
C5-20S[9]	C	203	203	1220	76	1.93	0.92	406.8	586.1	48.3	285
C5-40N[9]	C	203	203	1220	76	1.93	0.92	502.2	572.3	38.1	569
C5-40S[9]	C	203	203	1220	76	1.93	0.92	502.2	572.3	38.1	569
C1-1[10]	C	400	400	2800	50	2.14	0.63	459.5	497.0	24.9	450
C1-2[10]	C	400	400	2800	50	2.14	0.63	459.5	497.0	26.7	675

C1-3[10]	C	400	400	2800	50	2.14	0.63	459.5	497.0	26.1	900
C2-1[10]	C	400	400	2800	52	2.14	0.91	459.5	497.0	25.3	450
C2-2[10]	C	400	400	2800	52	2.14	0.91	459.5	497.0	27.1	675
C2-3[10]	C	400	400	2800	52	2.14	0.91	459.5	497.0	26.8	900
C3-1[10]	C	400	400	2800	54	2.14	0.59	459.5	497.0	26.4	450
C3-2[10]	C	400	400	2800	54	2.14	0.59	459.5	497.0	27.5	675
C3-3[10]	C	400	400	2800	54	2.14	0.59	459.5	497.0	26.9	900
L1[11]	C	400	400	3200	100	1.42	0.32	325.0	362.0	24.8	157
L2[11]	C	400	400	3200	100	1.42	0.32	325.0	362.0	24.8	157
L3[11]	C	400	400	3200	100	1.42	0.32	325.0	362.0	24.8	157
2D16RS[12]	DC	200	200	800	50	2.01	0.57	315.9	368.9	32.0	183
4D13RS[12]	DC	200	200	800	50	2.65	0.57	315.9	369.8	29.9	183
CA025C[13]	DC	200	200	600	70	2.36	1.21	426.1	361.6	26.3	265
CA060C[13]	DC	200	200	600	70	2.36	1.21	426.1	361.6	26.3	636
U1[14]	C	350	350	2000	150	3.21	0.30	470.0	430.0	43.6	0
U3[14]	C	350	350	2000	75	3.21	0.60	470.0	430.0	34.8	600
U4[14]	C	350	350	2000	50	3.21	0.90	470.0	438.0	32.0	600
U6[14]	C	350	350	2000	65	3.21	0.85	425.0	437.0	37.3	600
U7[14]	C	350	350	2000	65	3.21	0.85	425.0	437.0	39.0	600
1986, No. 1[15]	DE	400	400	3200	85	1.51	0.45	364.0	446.0	46.5	744
1986, No. 2[15]	DE	400	400	3200	78	1.51	0.64	360.0	446.0	44.0	2112
1986, No. 3[15]	DE	400	400	3200	91	1.51	0.42	364.0	446.0	44.0	2112
1986, No. 4[15]	DE	400	400	3200	94	1.51	0.30	255.0	446.0	40.0	1920
1990, No. 1[16]	DE	400	400	3200	80	1.57	1.06	333.0	474.0	25.6	819
1990, No. 2[16]	DE	400	400	3200	80	1.57	1.06	333.0	474.0	25.6	819

1990, No. 3[16]	DE	400	400	3200	80	1.57	1.41	333.0	474.0	25.6	819
1990, No. 4[16]	DE	400	400	3200	80	1.57	1.41	333.0	474.0	25.6	819
1990, No. 5[16]	C	550	550	3300	110	1.25	0.75	325.0	511.0	32.0	968
1990, No. 6[16]	C	550	550	3300	110	1.25	1.12	325.0	511.0	32.0	968
1990, No. 7[16]	C	550	550	3300	90	1.25	0.91	325.0	511.0	32.1	2913
1990, No. 8[16]	C	550	550	3300	90	1.25	1.37	325.0	511.0	32.1	2913
1986, No. 7[17]	DE	400	400	3200	117	1.51	1.01	466.0	440.0	28.3	1041
1986, No. 8[17]	DE	400	400	3200	92	1.51	1.28	466.0	440.0	40.1	2502

Footnotes: DC= double curvature, or with two fixed ends, SC=single curvature, or cantilever, b=width of the section, h= Depth of the section, L_{in}= length of the column from the inflection point to the end section, S_h= hoop spacing, ρ_g=longitudinal reinforcement ratio, ρ_w= transverse reinforcement ratio, f_{syx}= longitudinal reinforcement yield stress, f_{syy}= transverse reinforcement yield stress, f'_c= concrete compression strength , P=axial load, Failure mode 1: shear failure at crack $\varepsilon_2 < \varepsilon'_c$, Failure mode 2: loss of compression strength $\varepsilon_2 < \varepsilon'_c$, and Failure mode 3: shear-compression failure $\varepsilon_2 = \varepsilon'_c$, Test results by: [1]Amitsu et al. (1991), [2]Arakawa et al. (1982), [3]Arakawa et al. (1989), [4]Azizinamini et al. (1988), [5]Bett et al. (1985), Ghee et al. (1981), [7]Kono and Watanabe (2002), [8]Kono et al. (2003), [9]Matamoros et al. (1999), [10]Mo and Wang (2000), [11]Ohno and Nishioka (1984), [12]Ohue et al. (1985), [13]Ono et al. (1989), [14]Saatcioglu and Ozcebe (1989), [15]Soesianawati et al. (1986), [16]Tanaka and Park (1990), [17]Zahn et al. (1986)

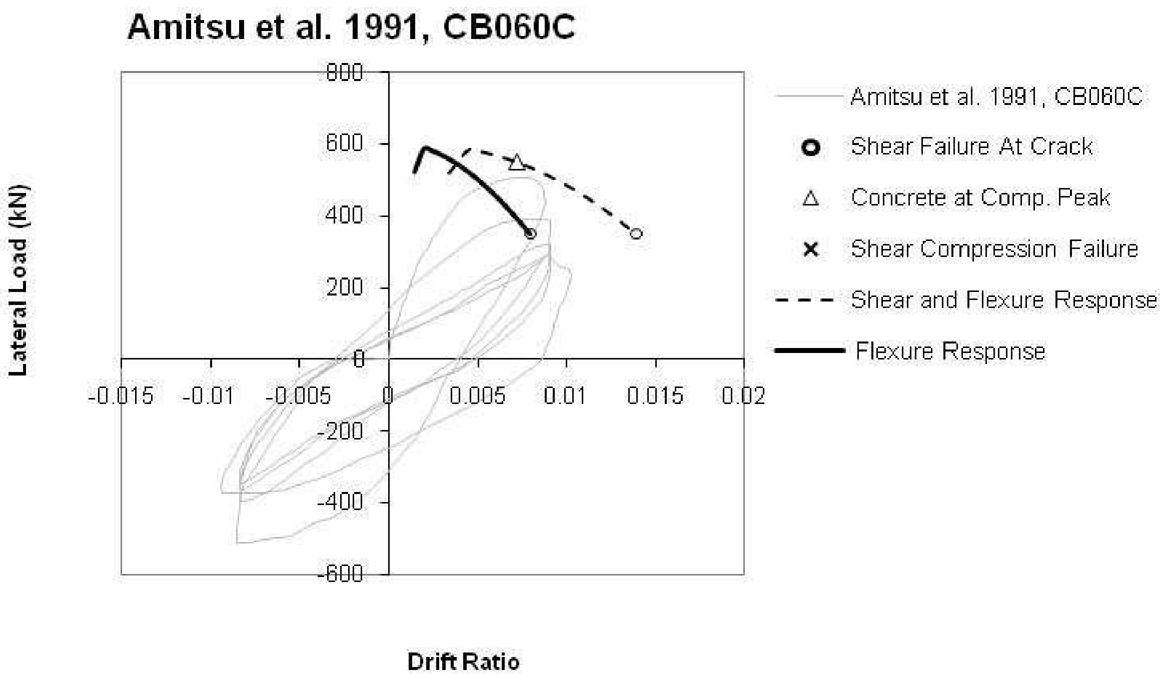

Figure 5. Amitsu et al. 1991, CB060C.

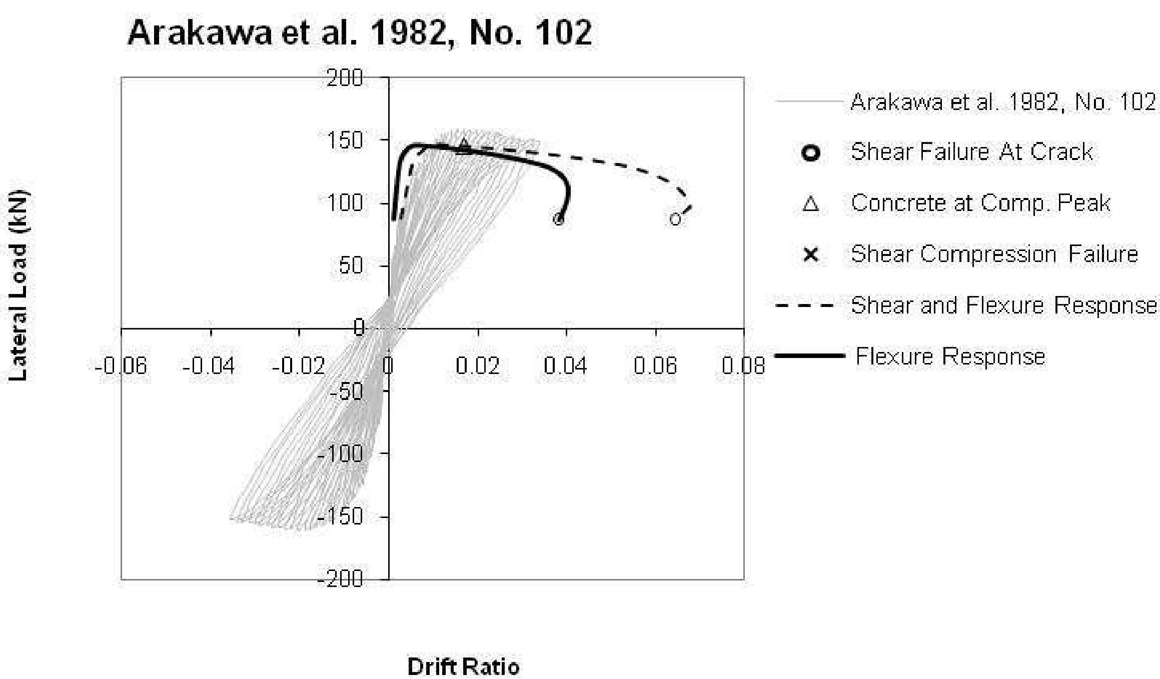

Figure 6. Arakawa et al. 1982, No 102.

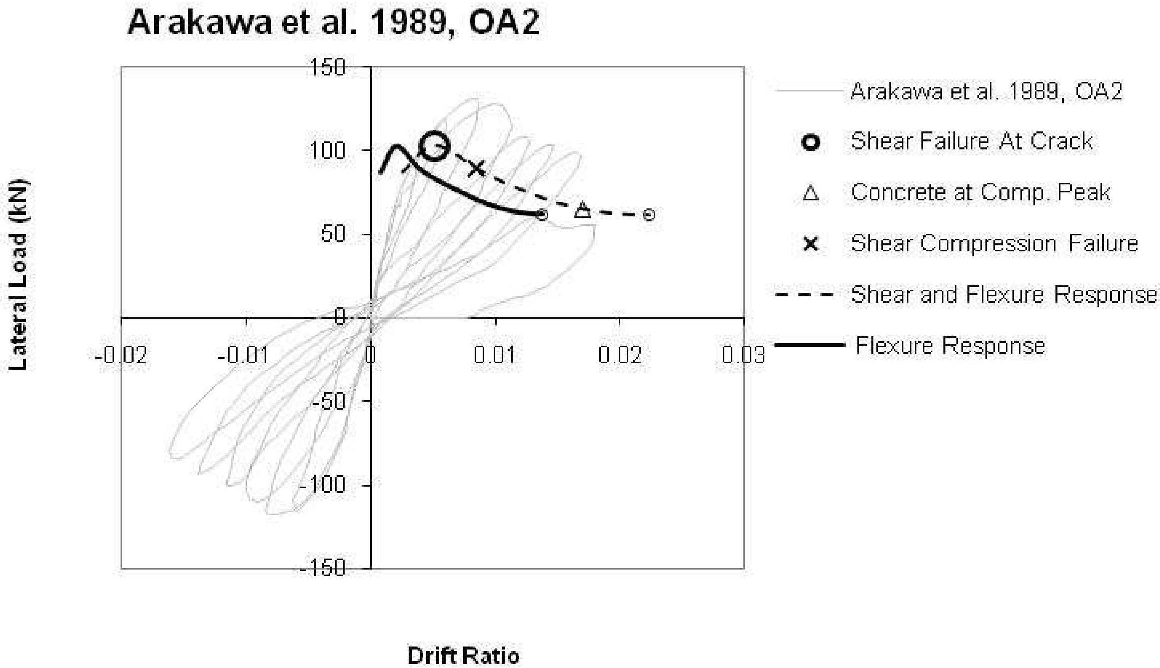

Figure 7. Arakawa et al. 1989, OA2.

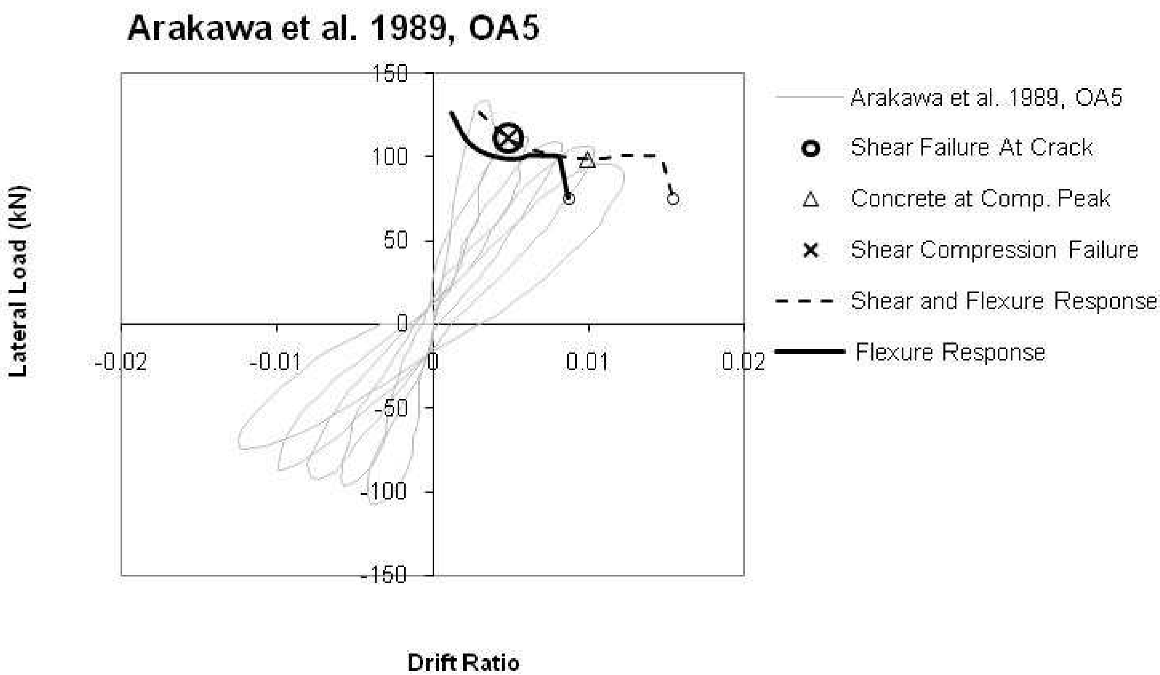

Figure 8. Arakawa et al. 1989, OA5.

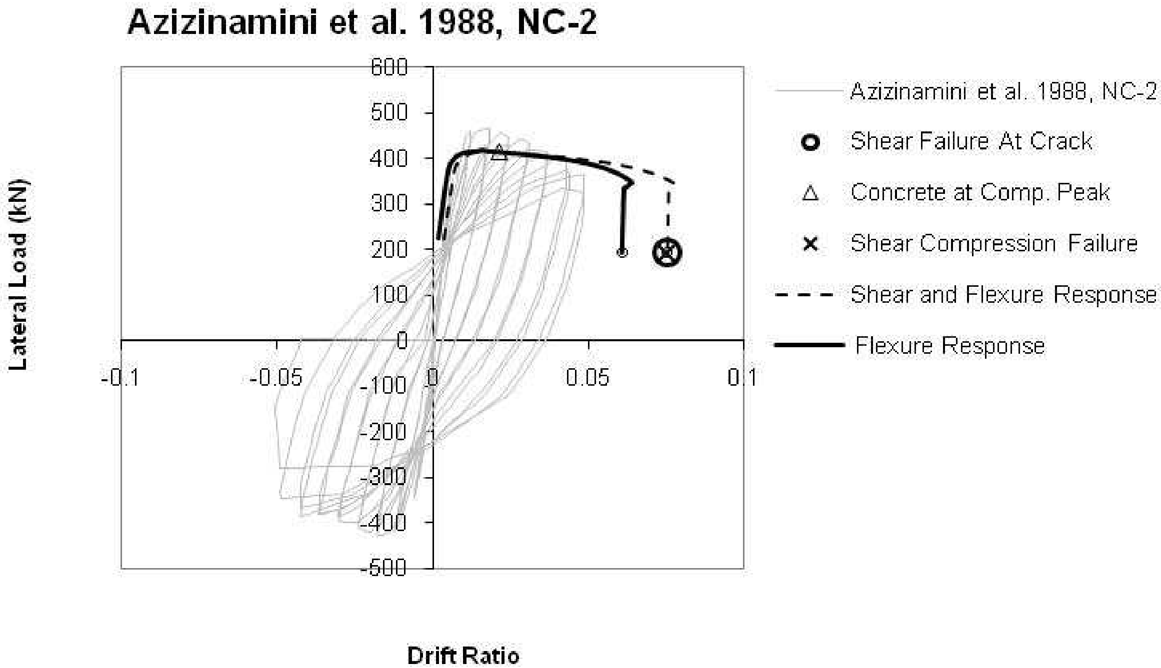

Figure 9. Azizinamini et al. 1988, NC-2.

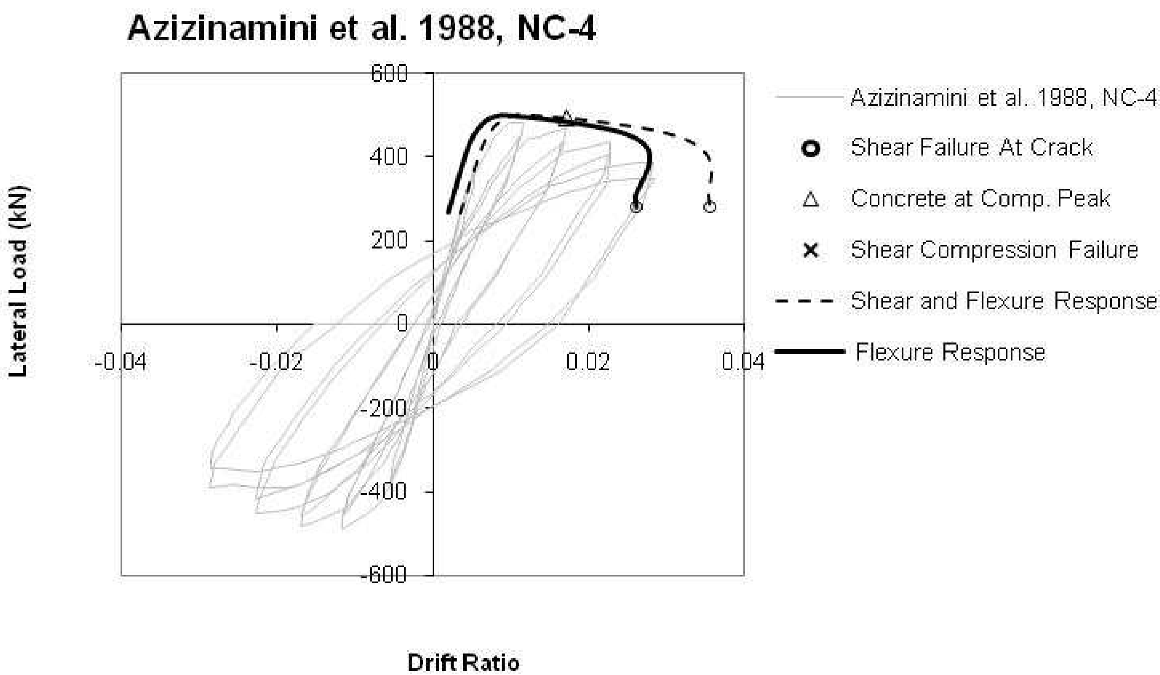

Figure 10. Azizinamini et al. 1988, NC-4.

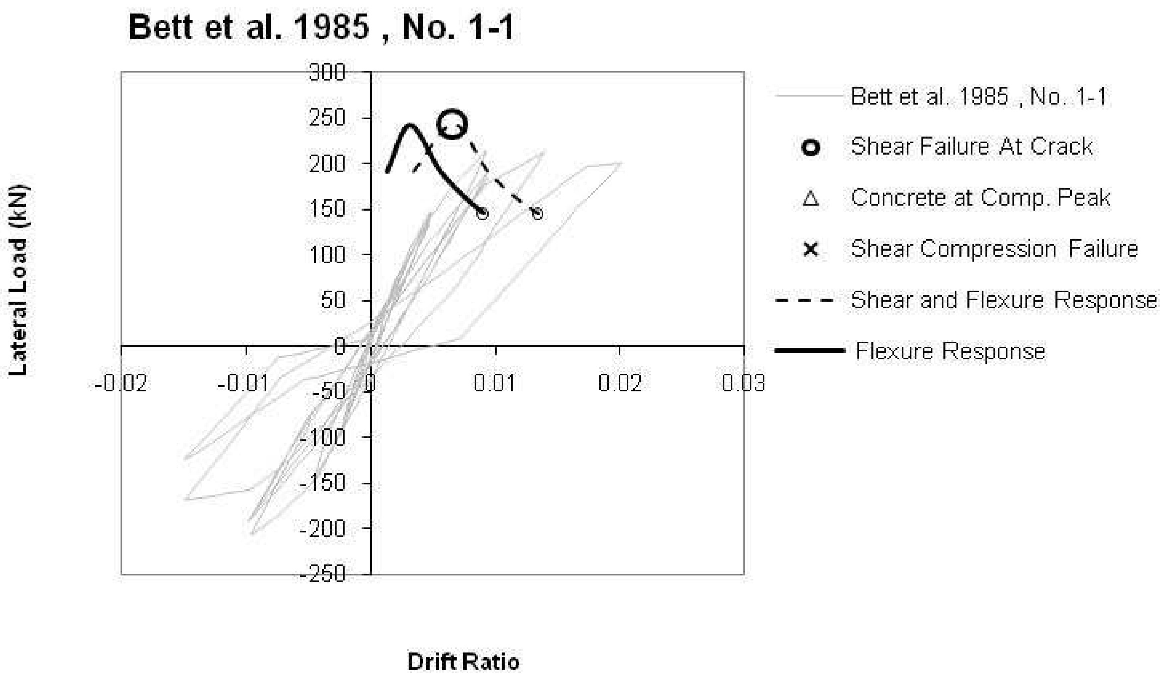

Figure 11. Bett et al. 1985, No. 1-1.

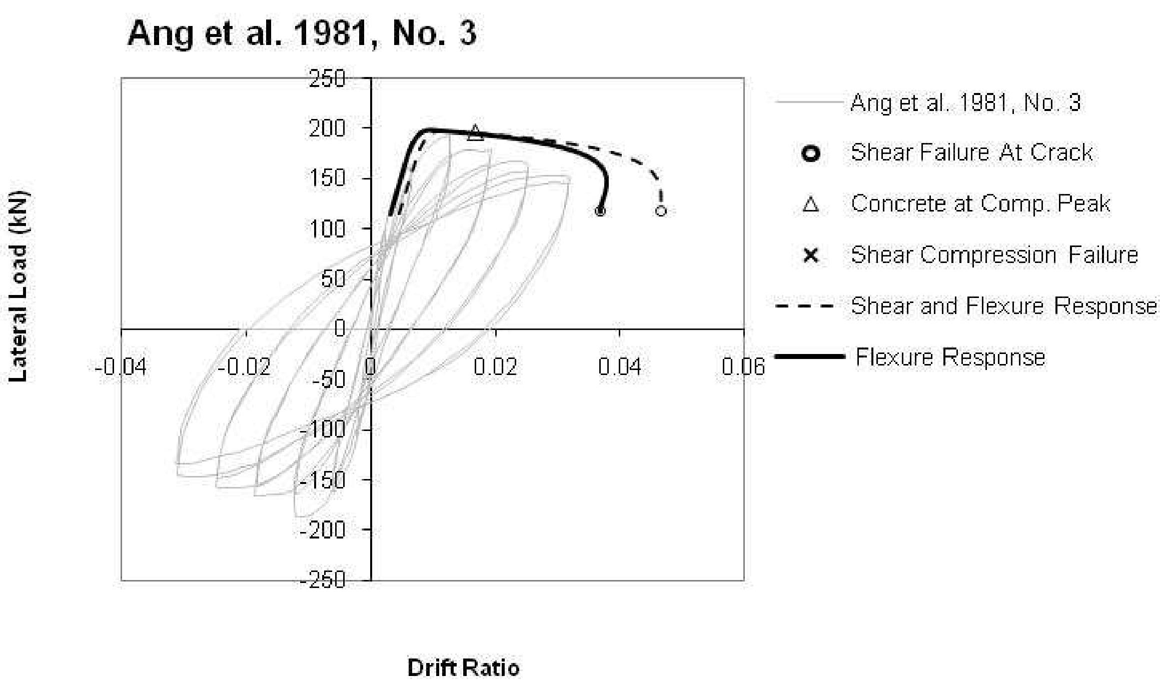

Figure 12. Ang et al. 1981, No. 3.

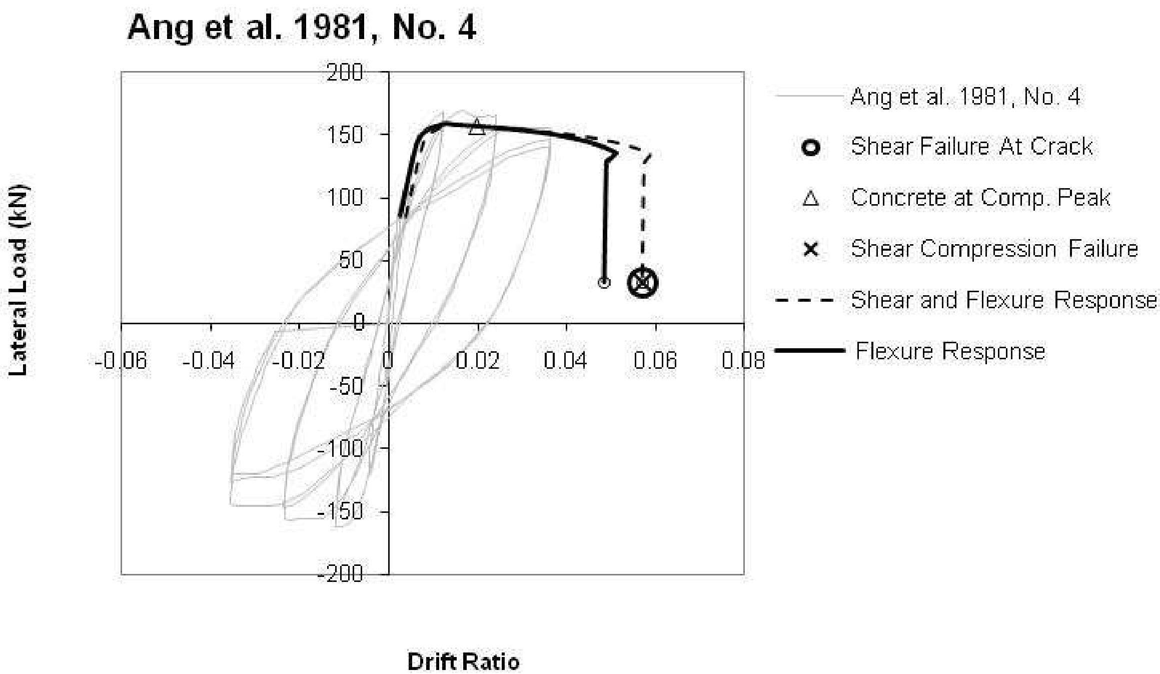

Figure 13. Ang et al. 1981, No. 4.

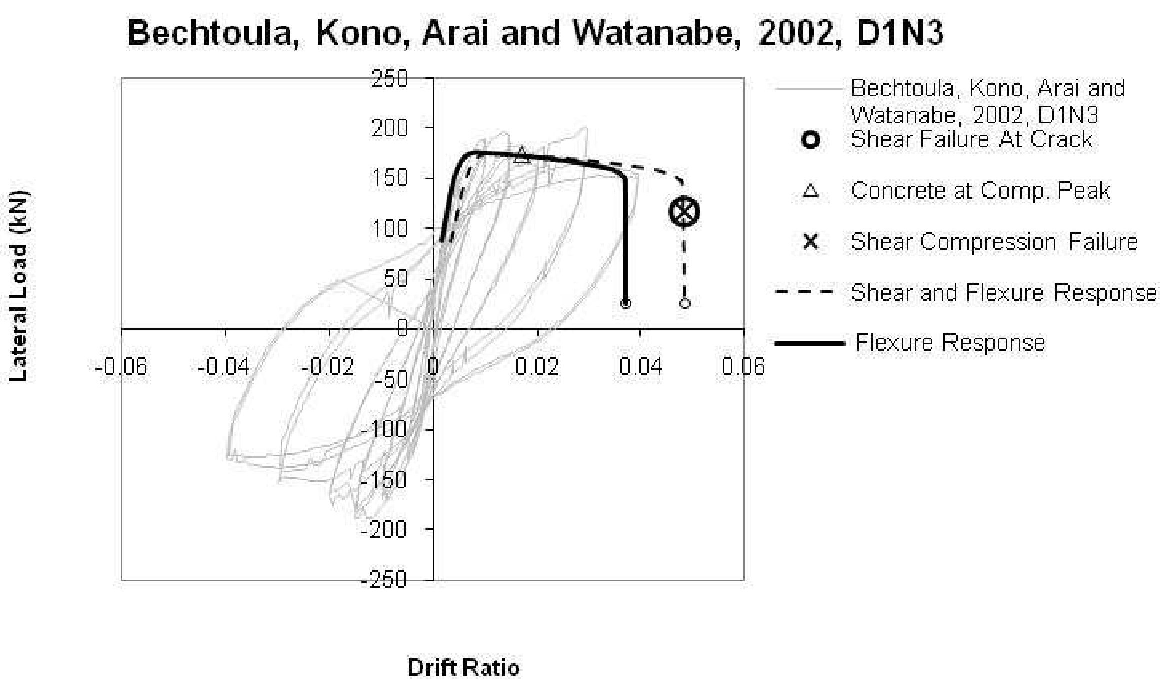

Figure 14. Bechtoula, Kono, Arai and Watanabe, 2002, D1N3.

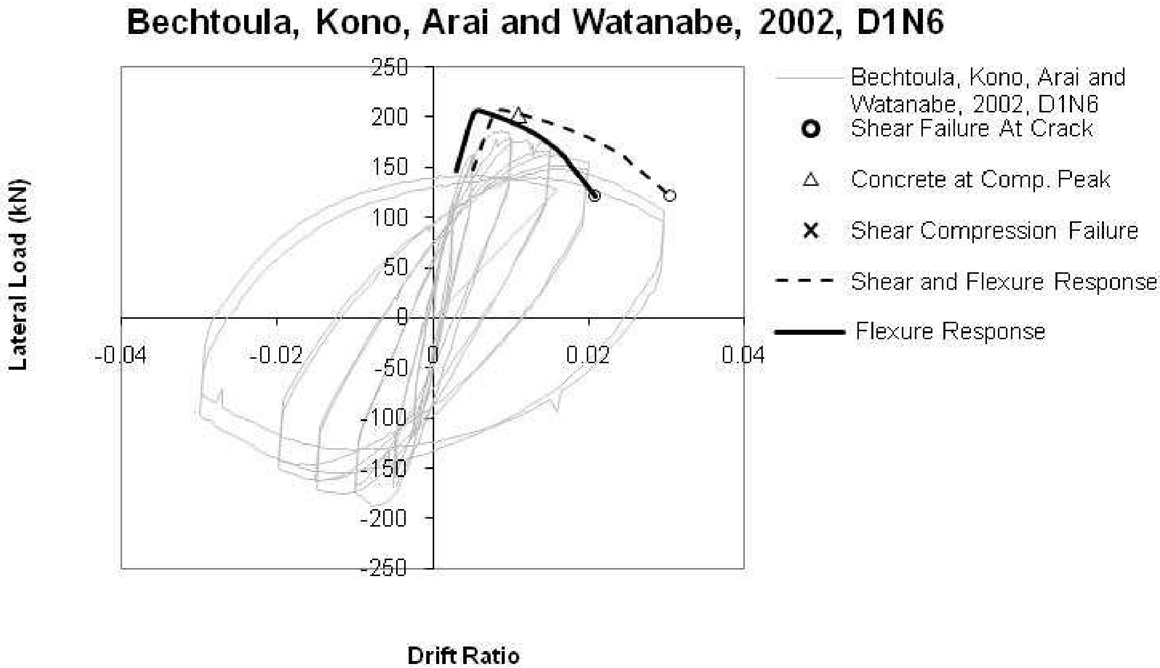

Figure 15. Bechtoula, Kono, Arai and Watanabe, 2002, D1N6.

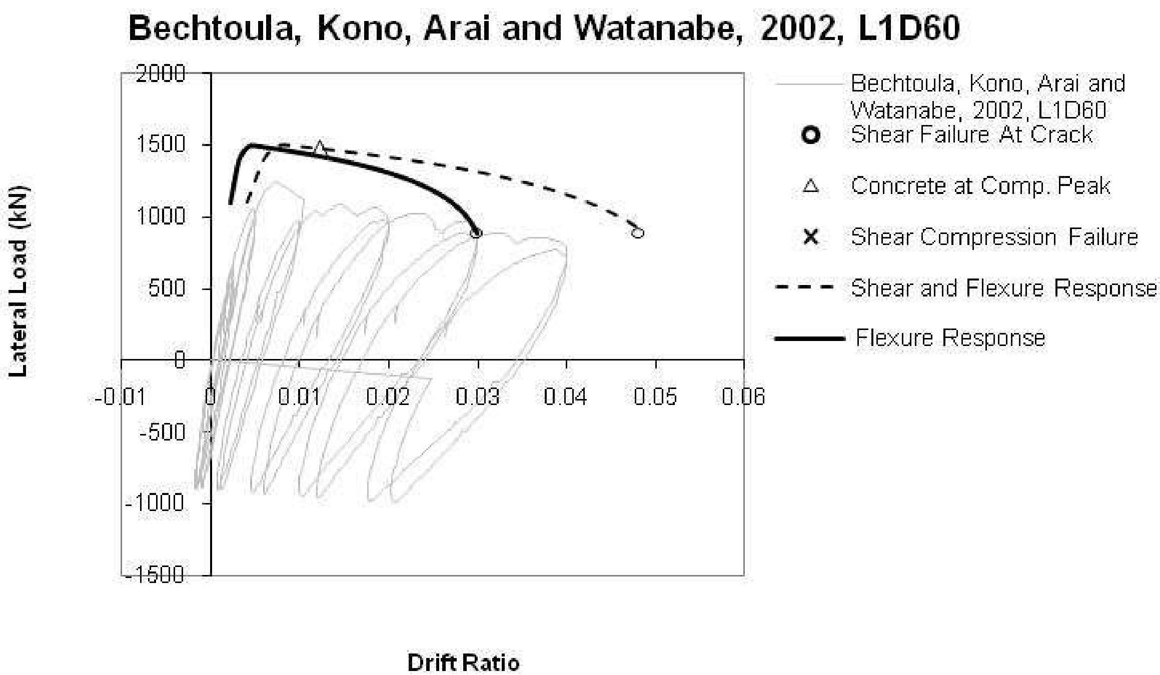

Figure 16. Bechtoula, Kono, Arai and Watanabe, 2002, L1D60.

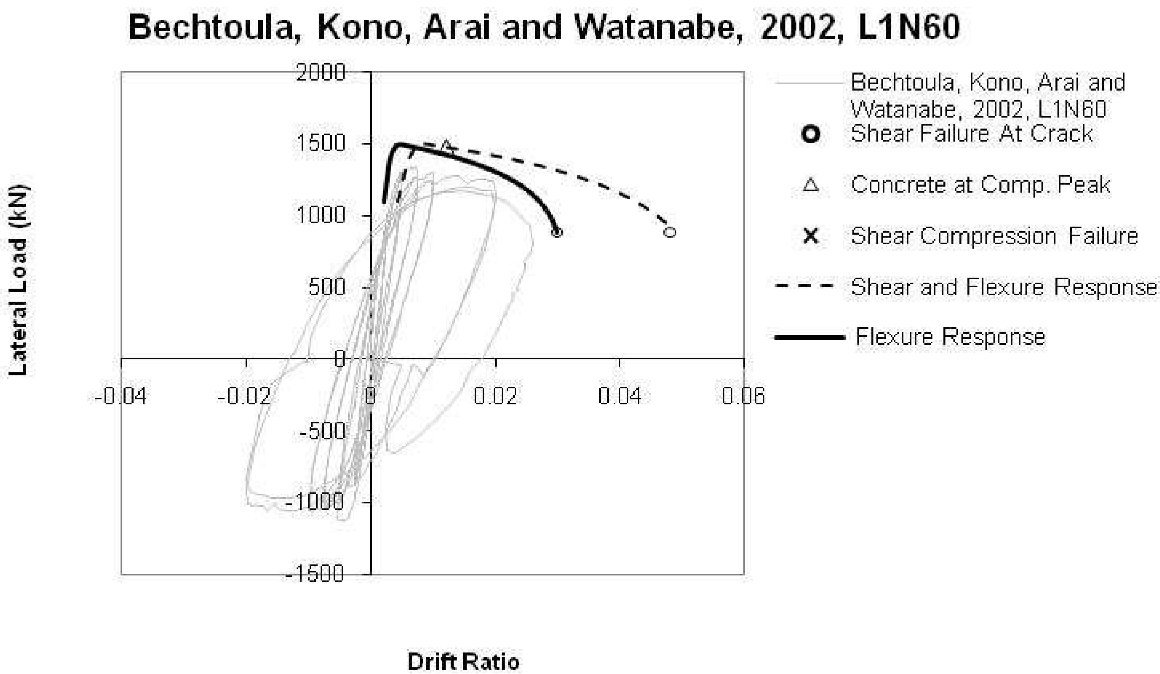

Figure 17. Bechtoula, Kono, Arai and Watanabe, 2002, L1N60.

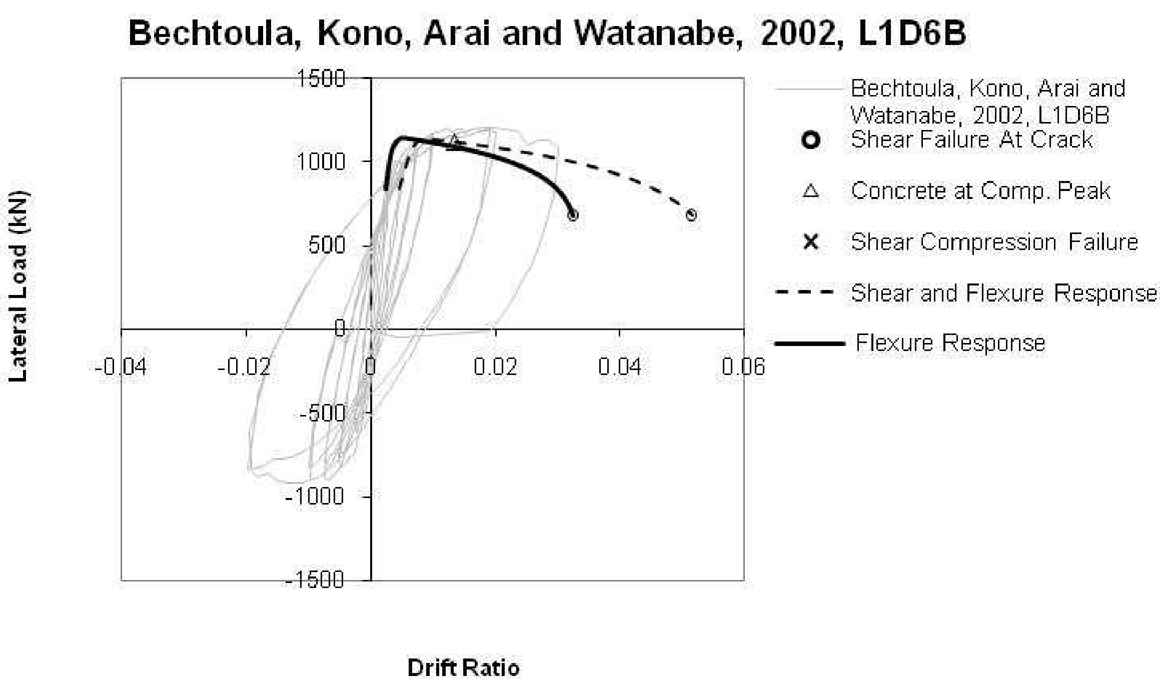

Figure 18. Bechtoula, Kono, Arai and Watanabe, 2002, L1D6B.

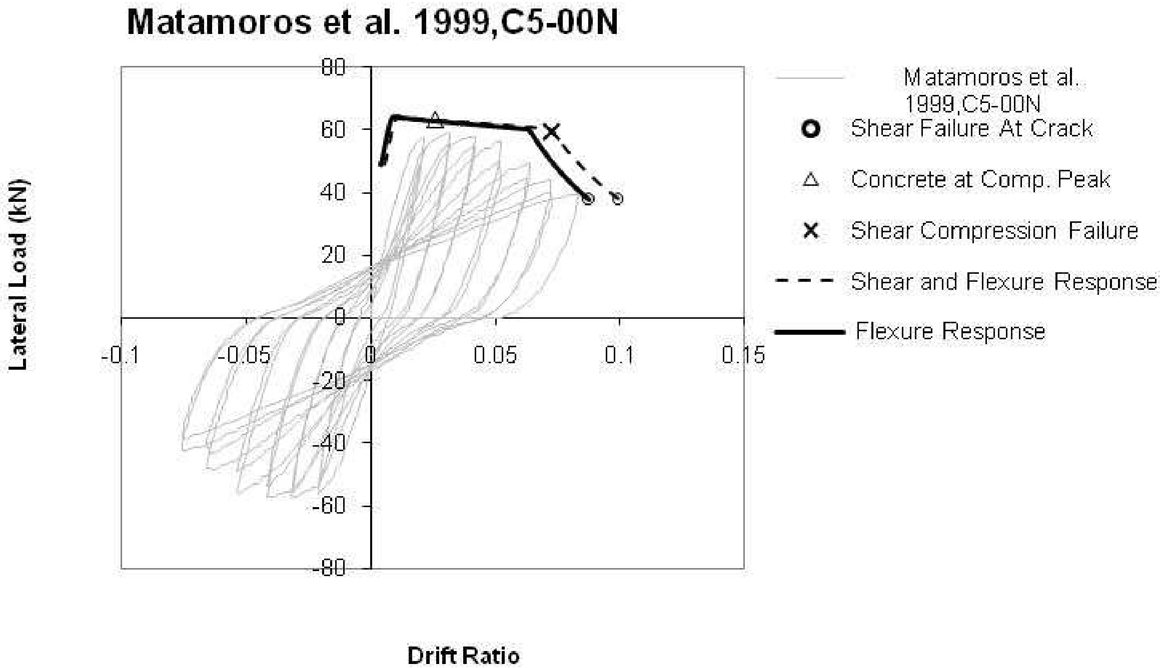

Figure 19. Matamoros et al. 1999, C5-00N.

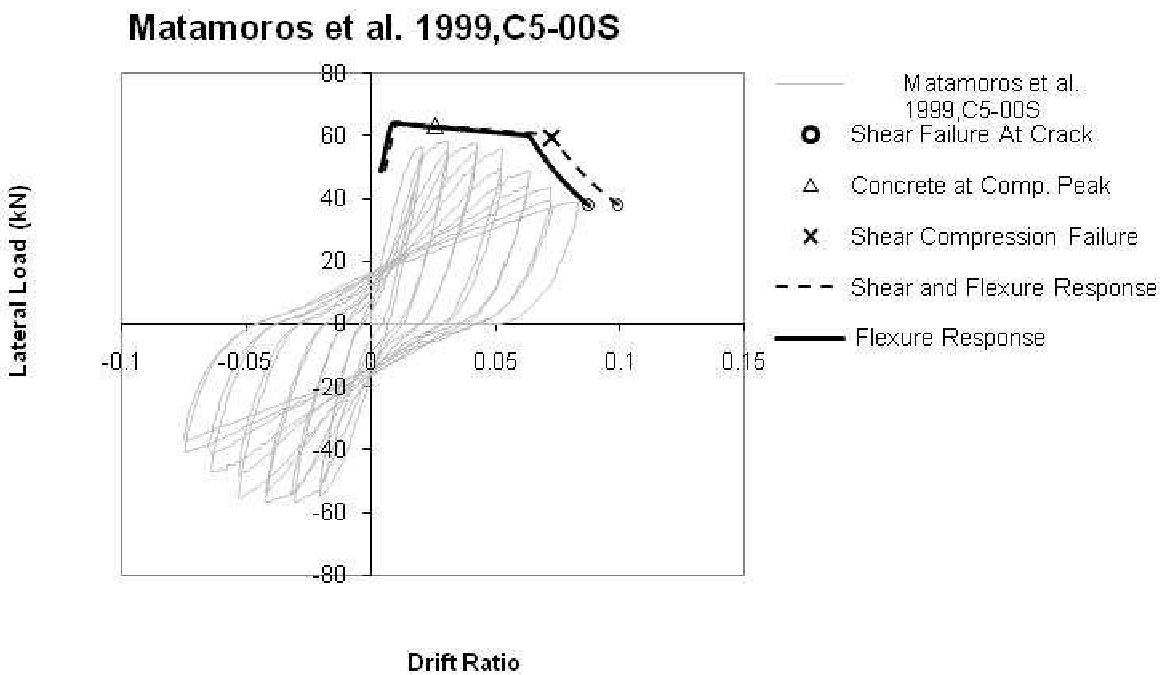

Figure 20. Matamoros et al. 1999, C5-00S.

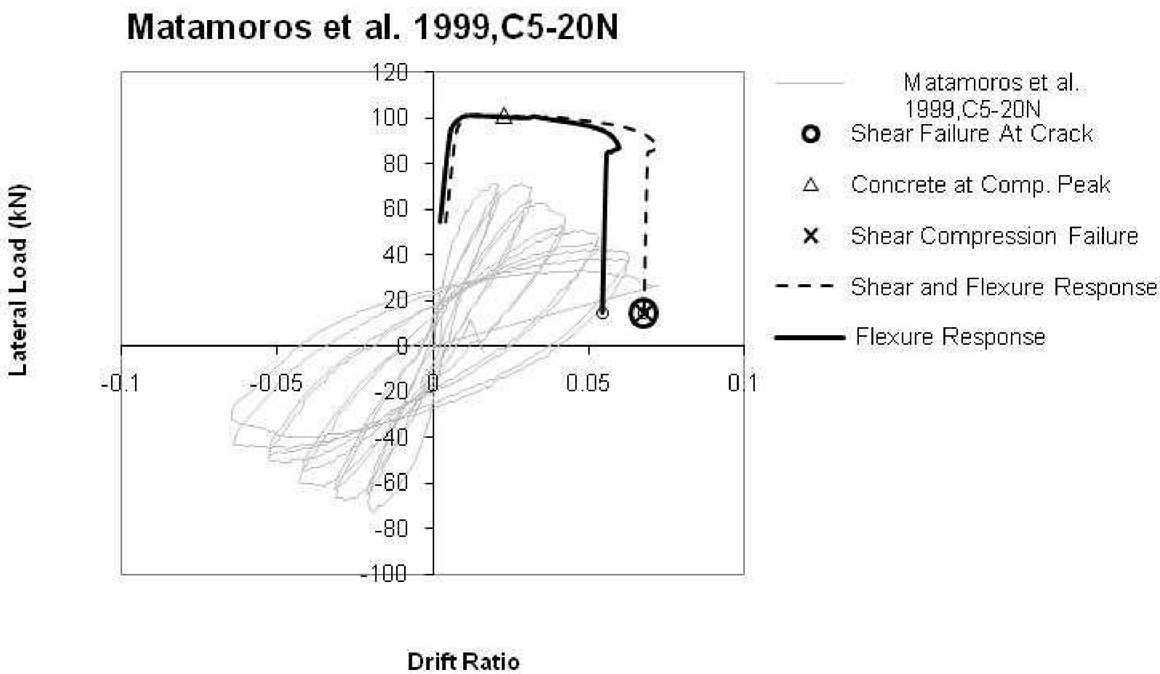

Figure 21. Matamoros et al. 1999, C5-20N.

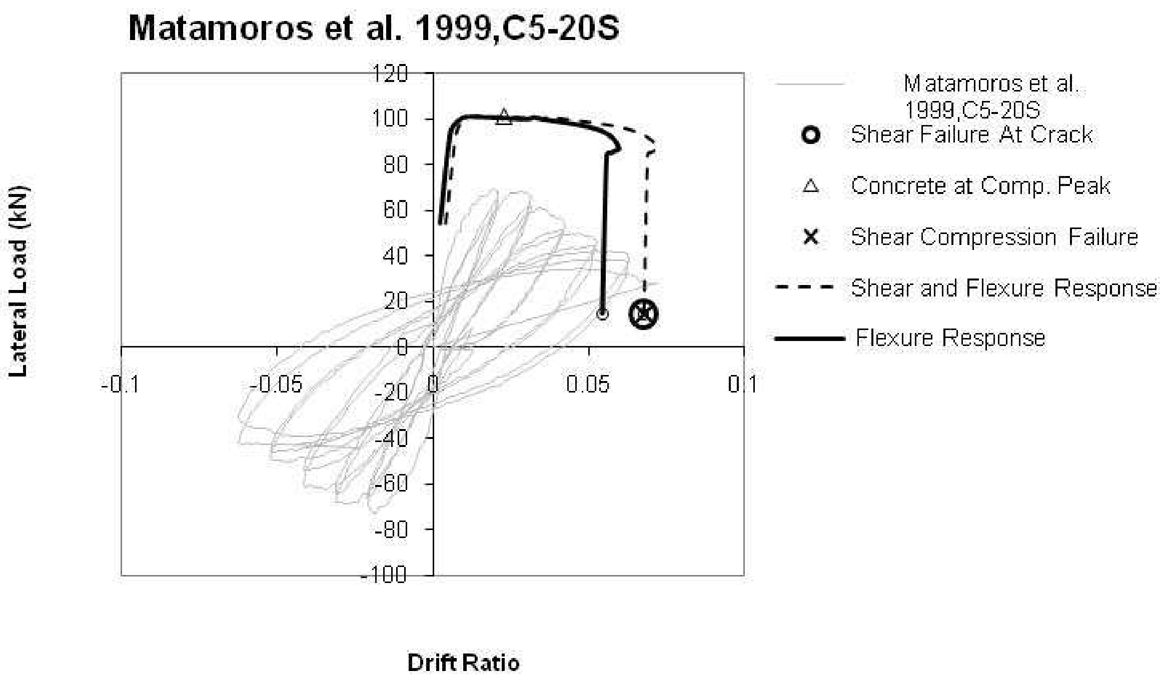

Figure 22. Matamoros et al. 1999, C5-20S.

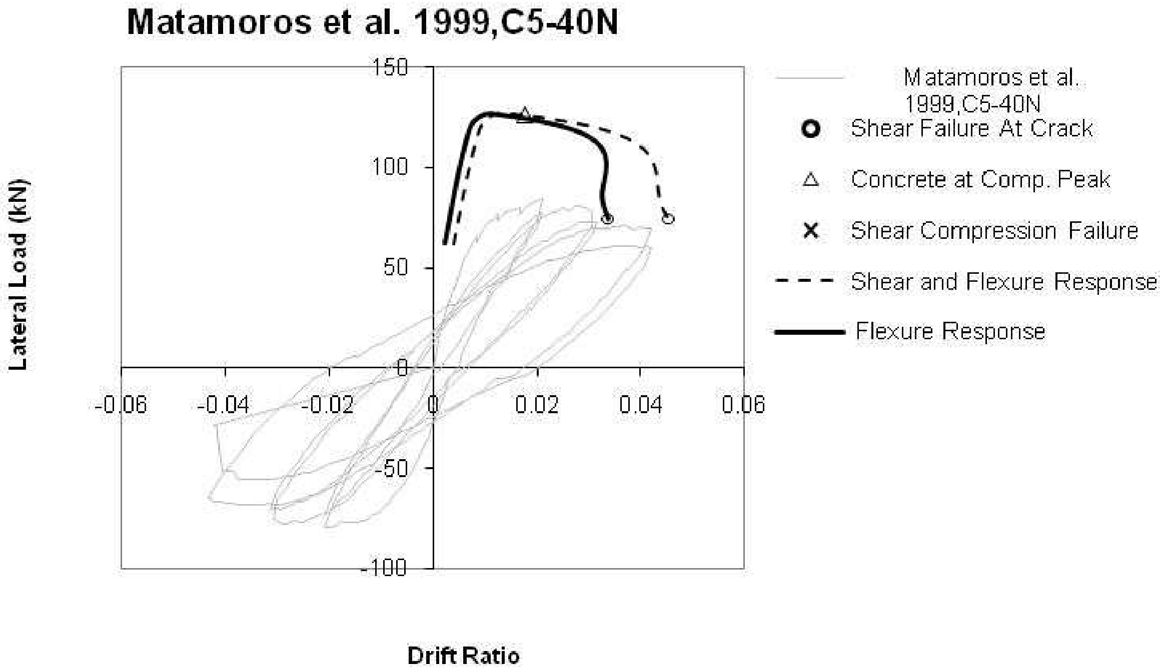

Figure 23. Matamoros et al. 1999, C5-40N.

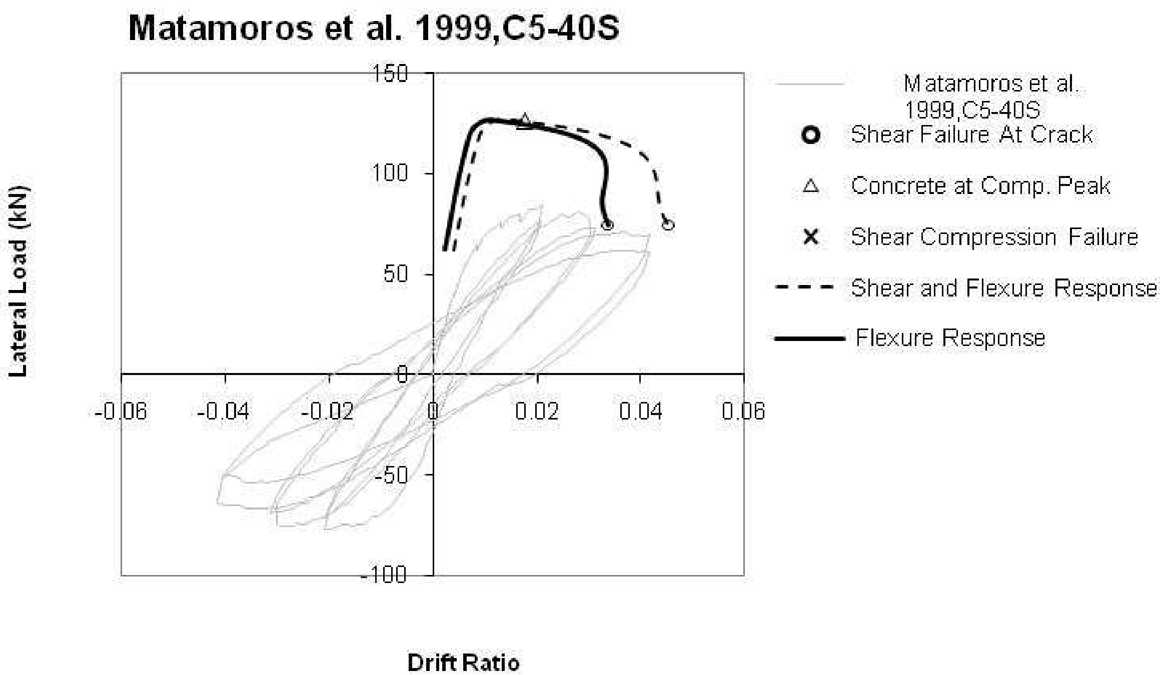

Figure 24. Matamoros et al. 1999, C5-40S.

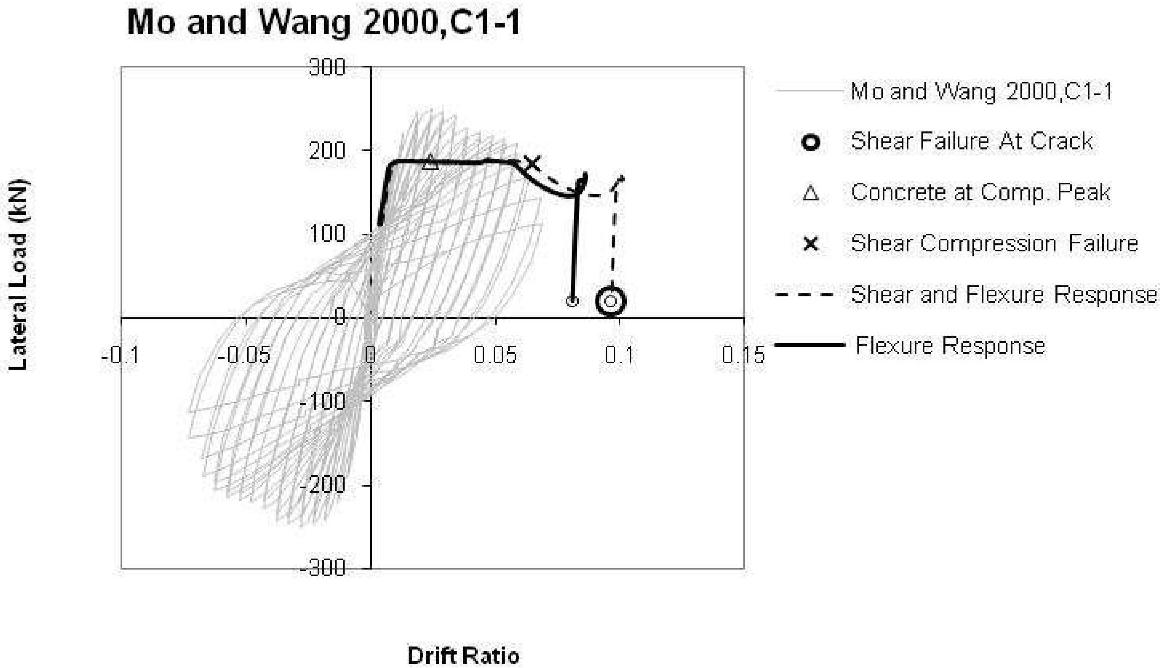

Figure 25. Mo and Wang 2000, C1-1.

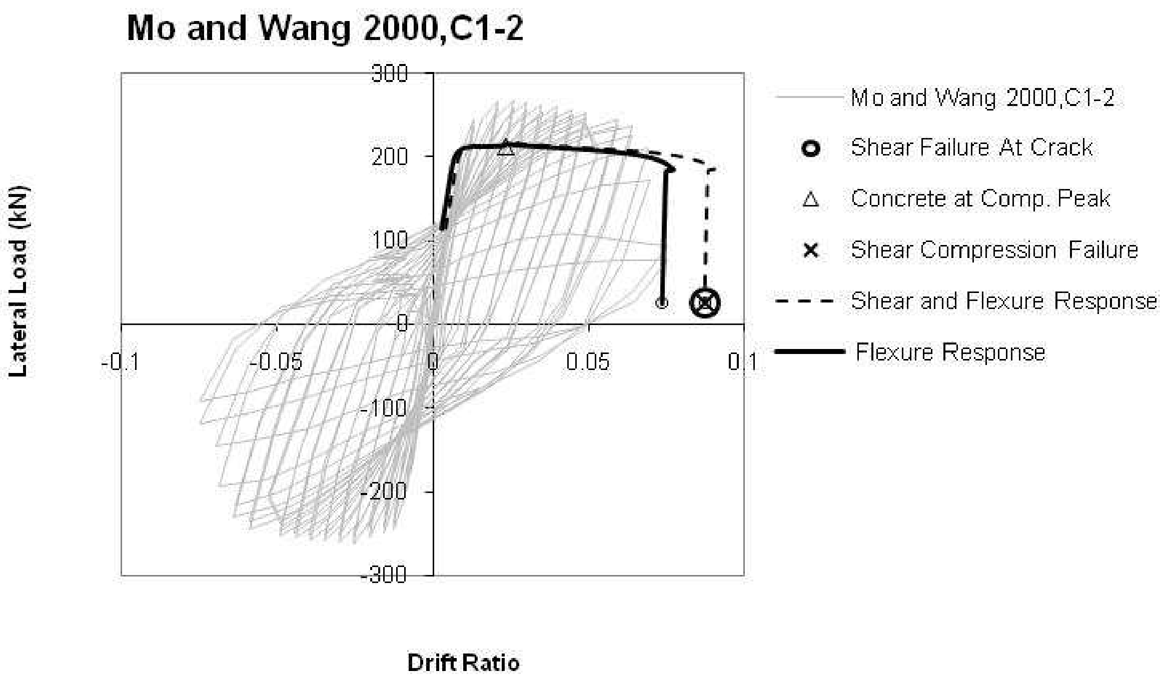

Figure 26. Mo and Wang 2000, C1-2.

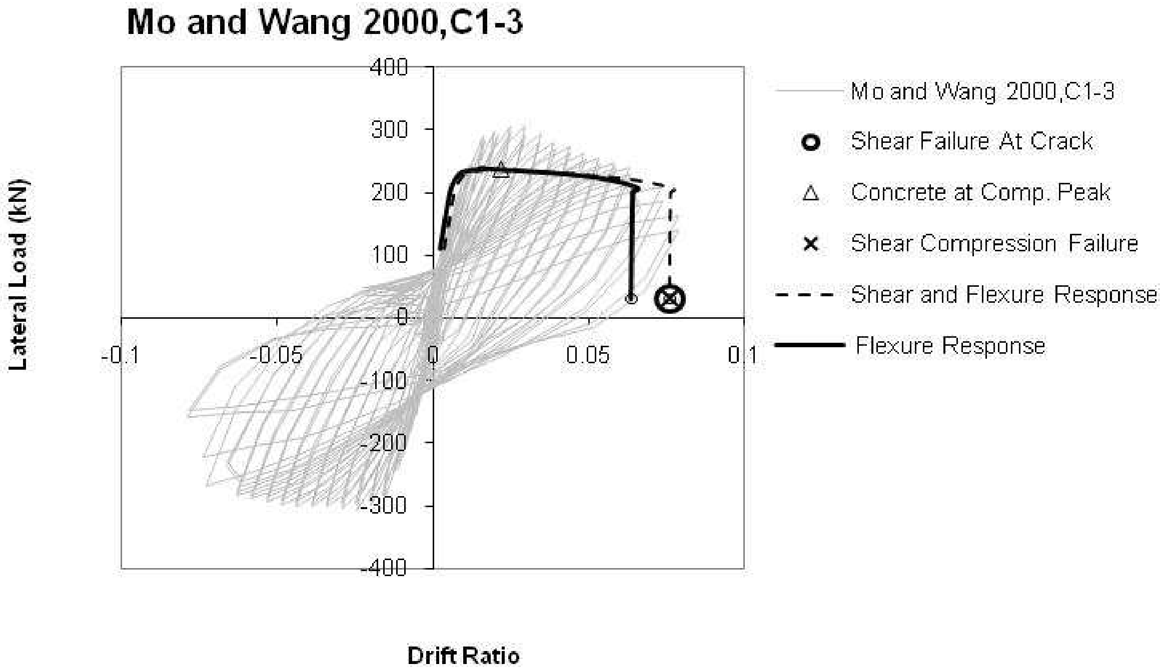

Figure 27. Mo and Wang 2000, C1-3.

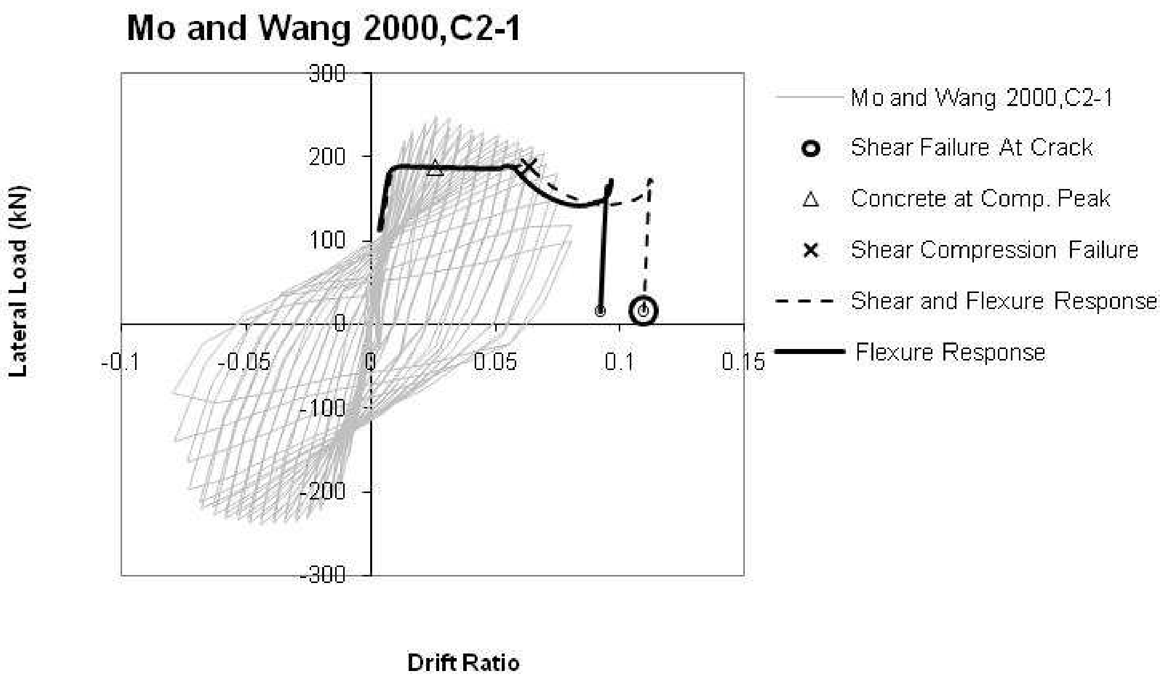

Figure 28. Mo and Wang 2000, C2-1.

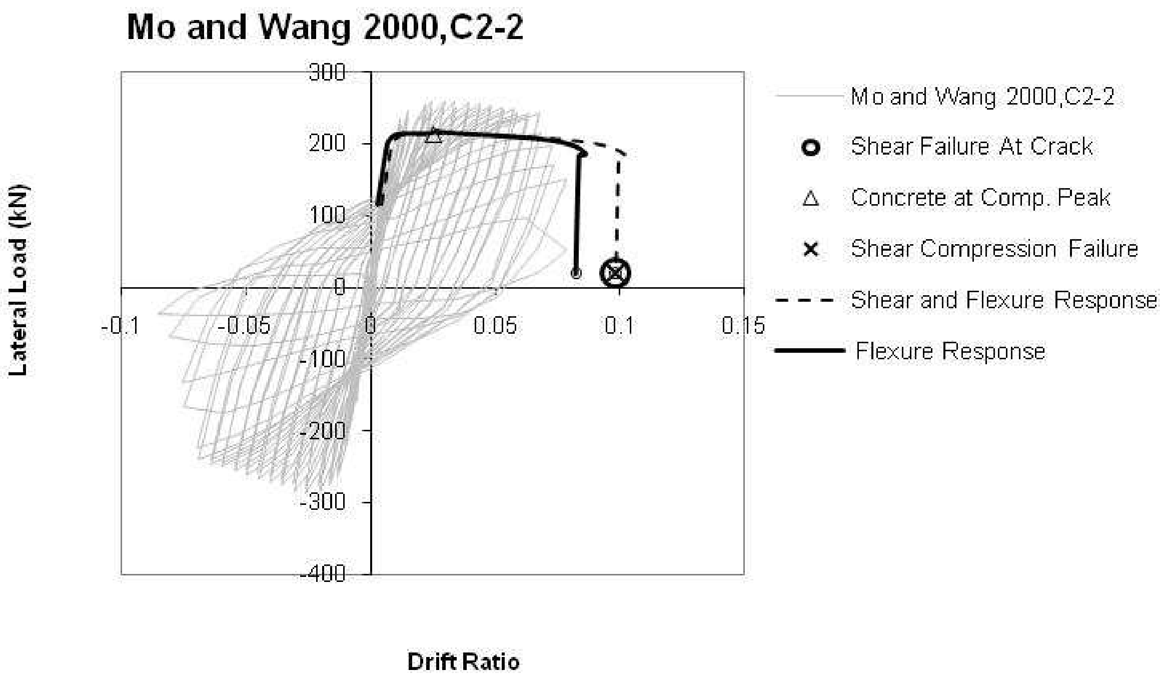

Figure 29. Mo and Wang 2000, C2-2.

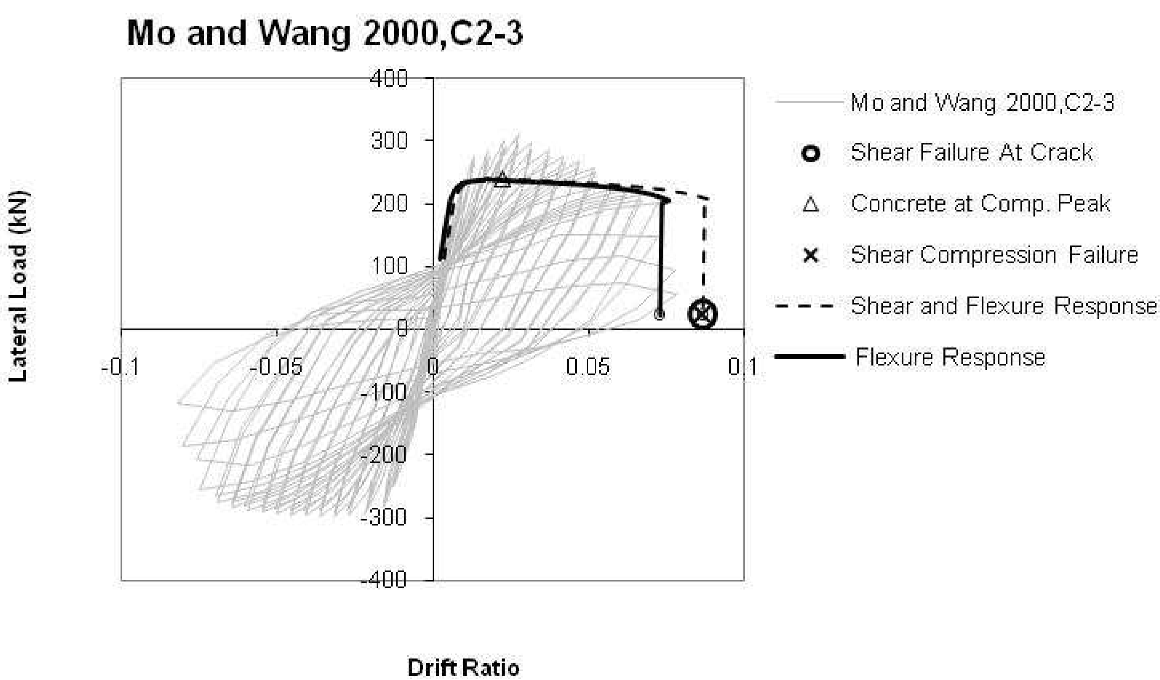

Figure 30. Mo and Wang 2000, C2-3.

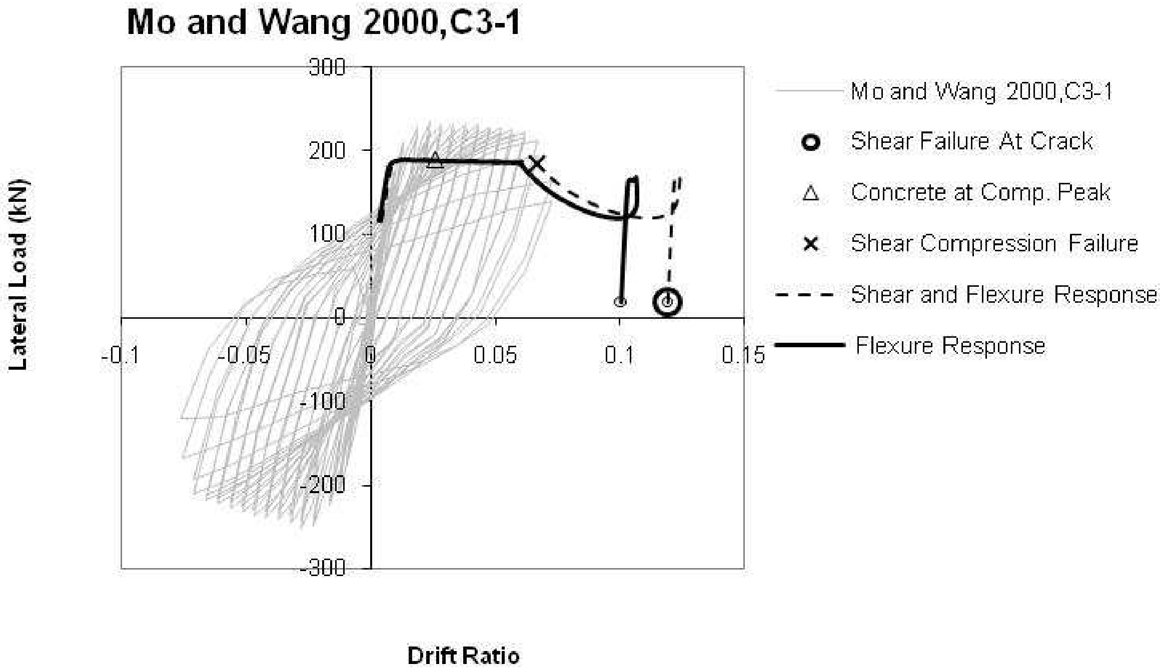

Figure 31. Mo and Wang 2000, C3-1.

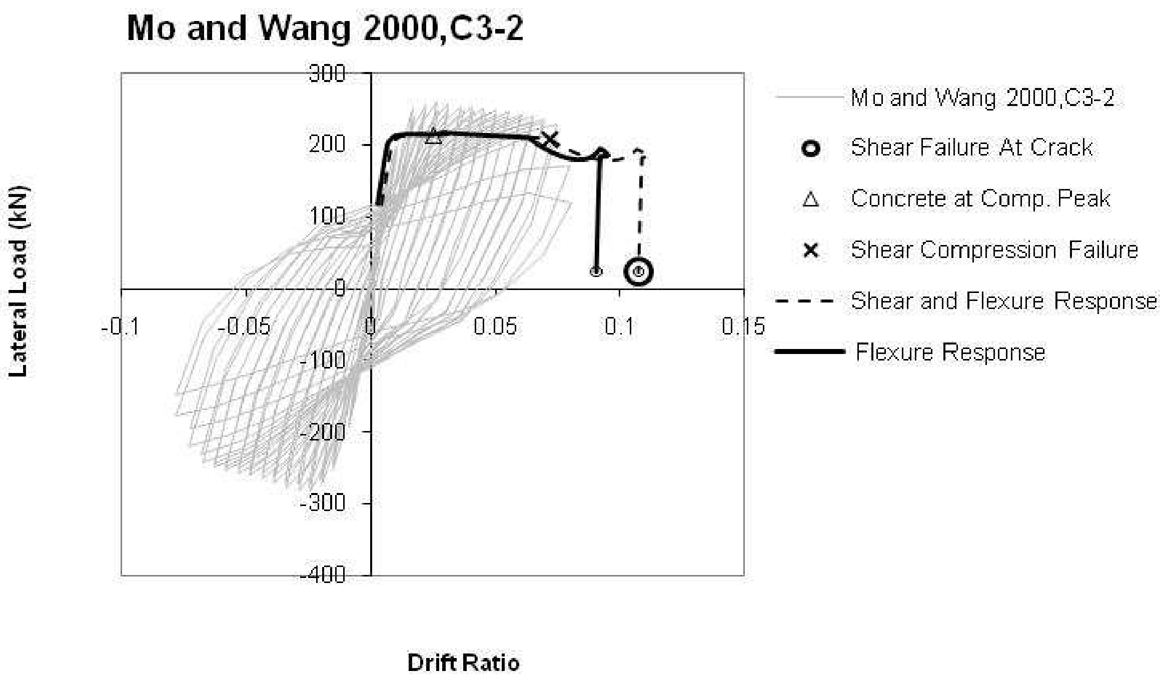

Figure 32. Mo and Wang 2000, C3-2.

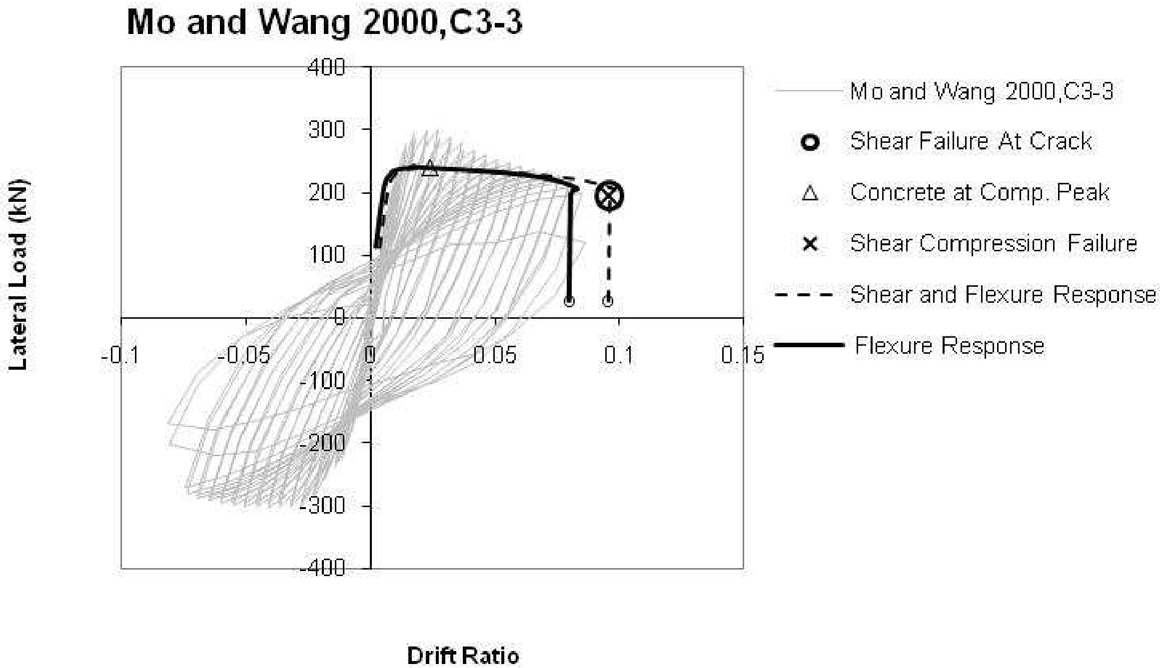

Figure 33. Mo and Wang 2000, C3-3.

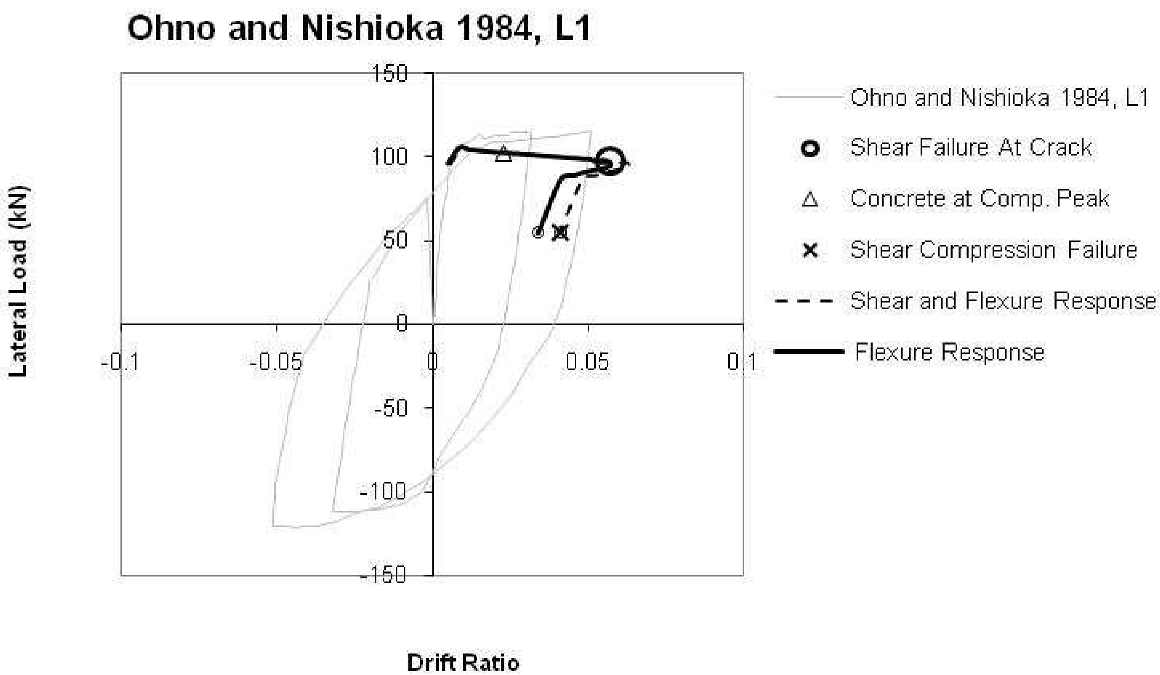

Figure 34. Ohno and Nishioka 1984, L1.

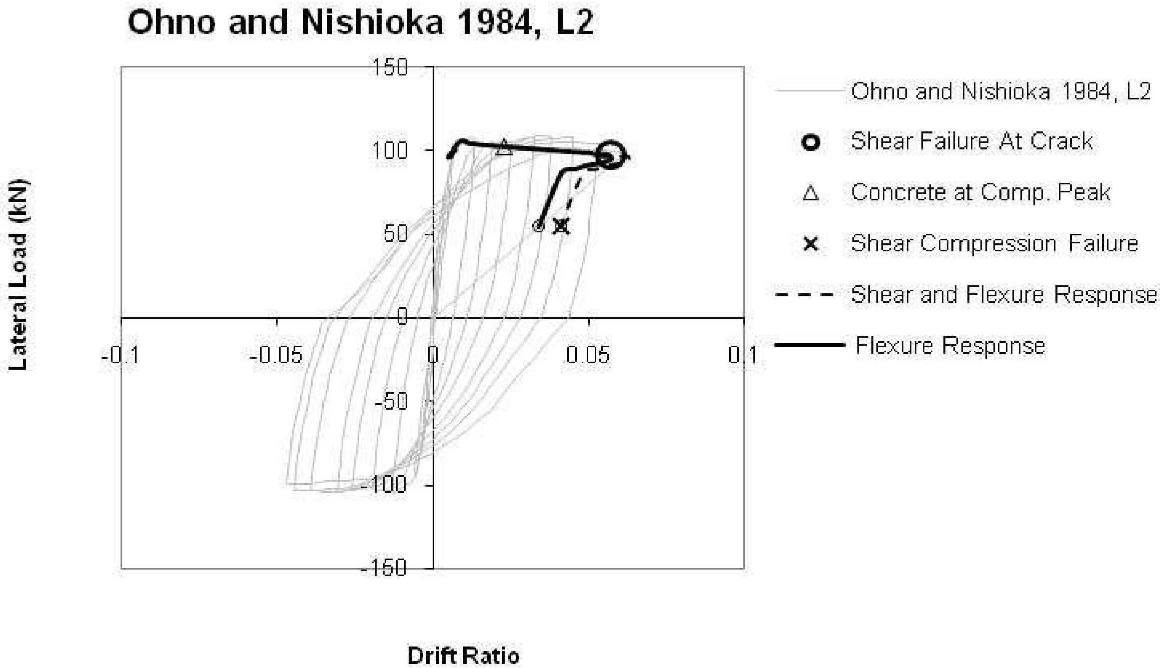

Figure 35. Ohno and Nishioka 1984, L2.

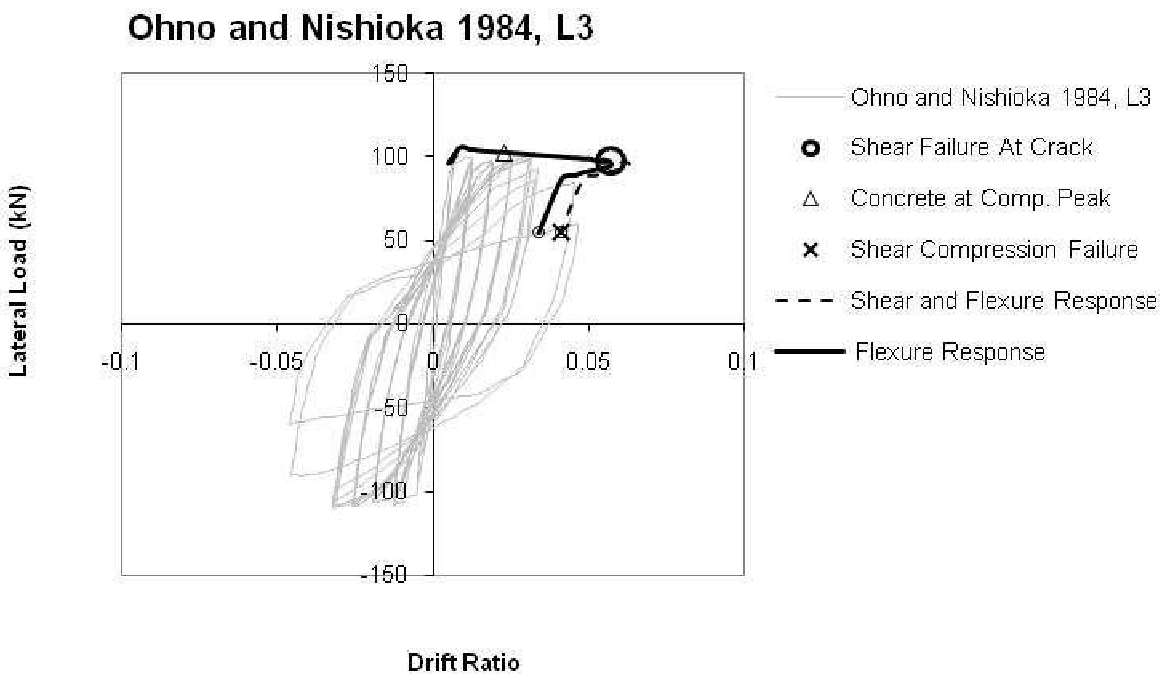

Figure 36. Ohno and Nishioka 1984, L3.

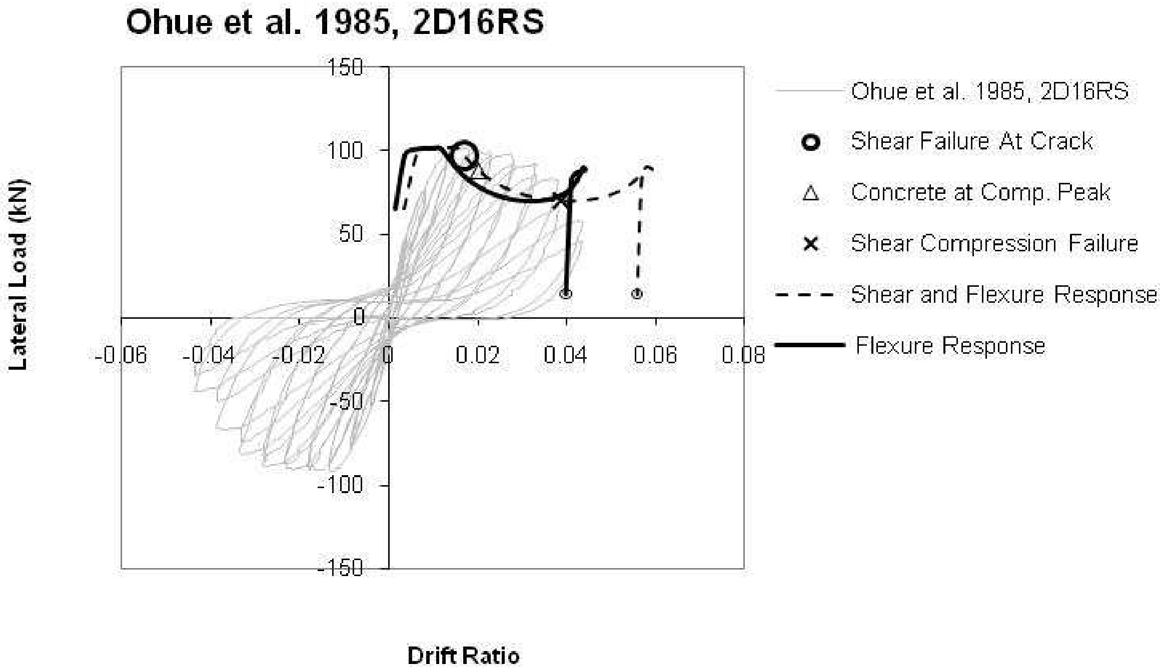

Figure 37. Ohue et al. 1985, 2D16RS.

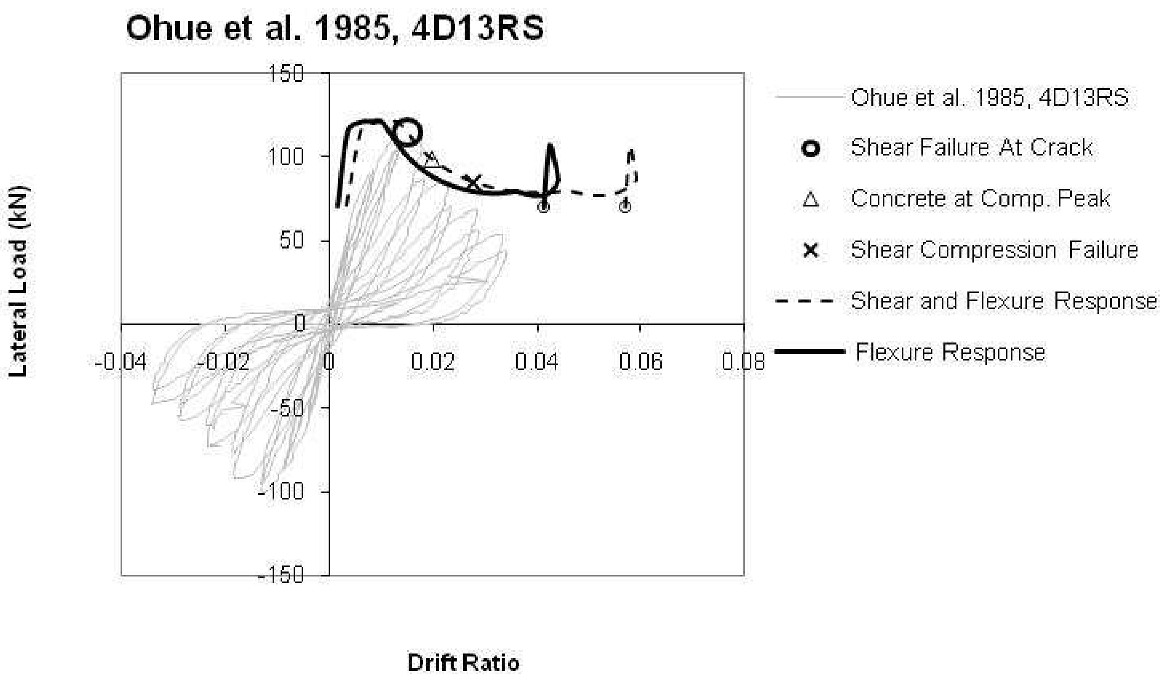

Figure 38. Ohue et al. 1985, 4D13RS.

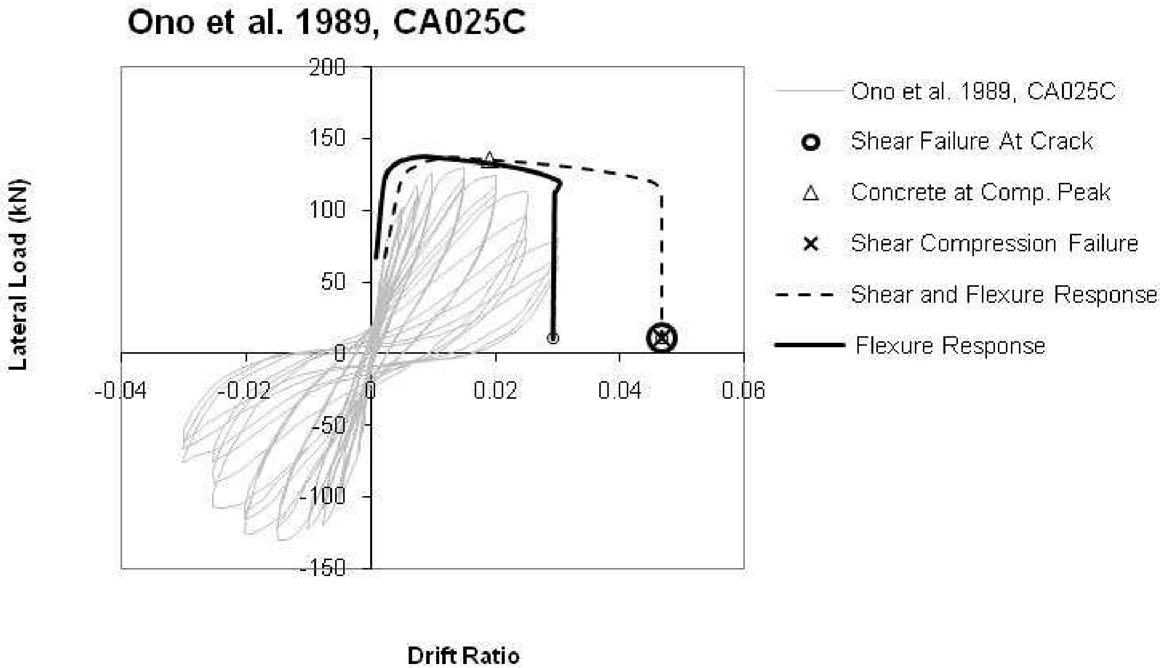

Figure 39. Ono et al. 1989, CA025C.

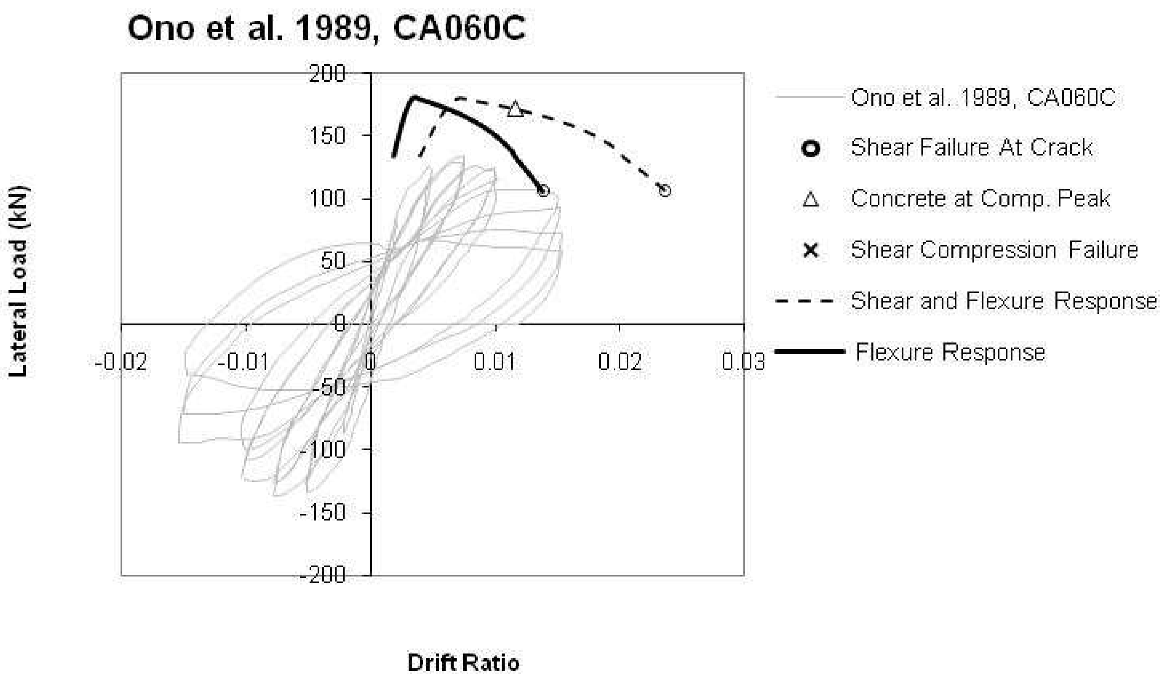

Figure 40. Ono et al. 1989, CA060C.

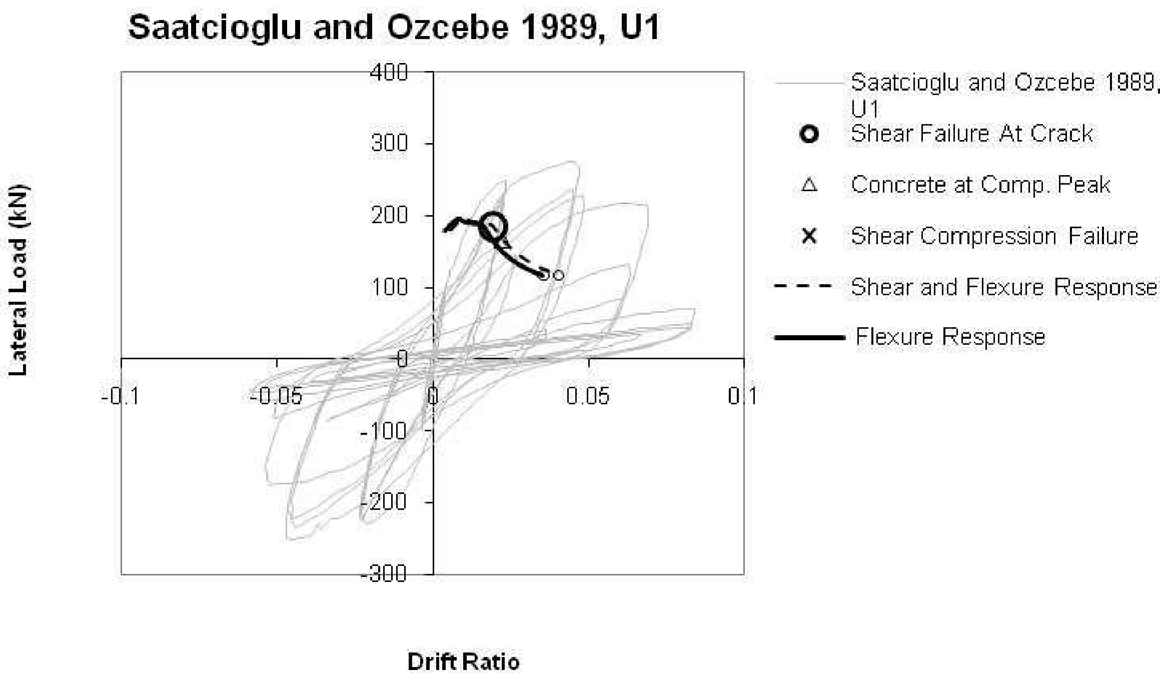

Figure 41. Saatcioglu and Ozcebe 1989, U1.

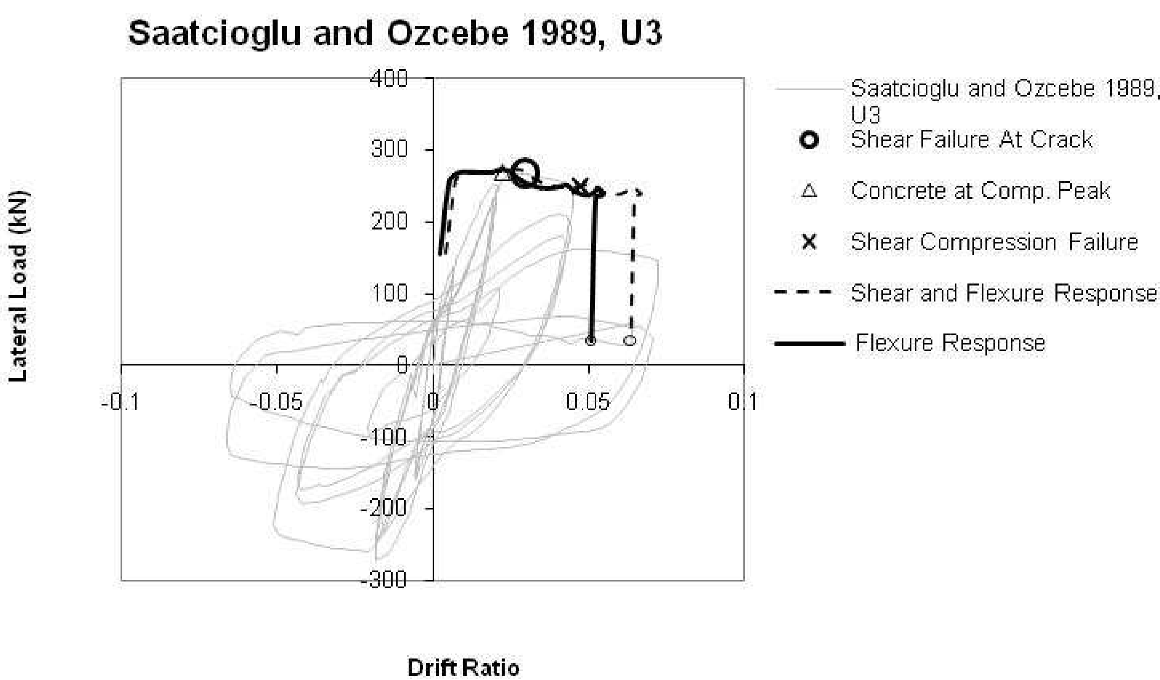

Figure 42. Saatcioglu and Ozcebe 1989, U3.

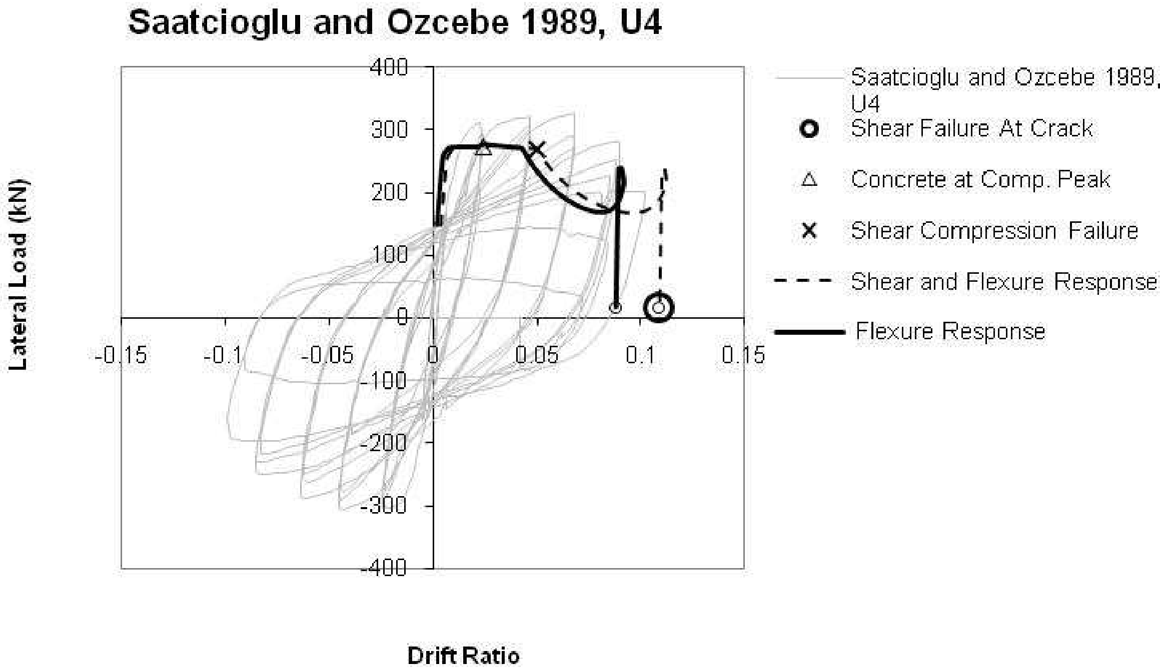

Figure 43. Saatcioglu and Ozcebe 1989, U4.

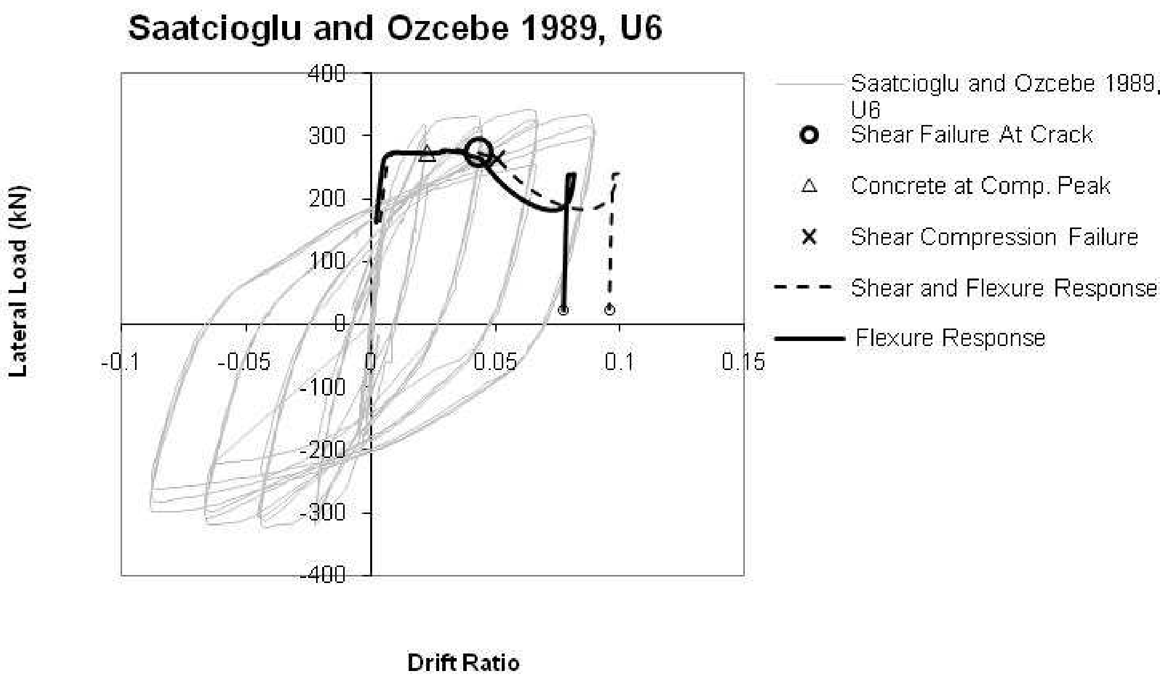

Figure 44. Saatcioglu and Ozcebe 1989, U6.

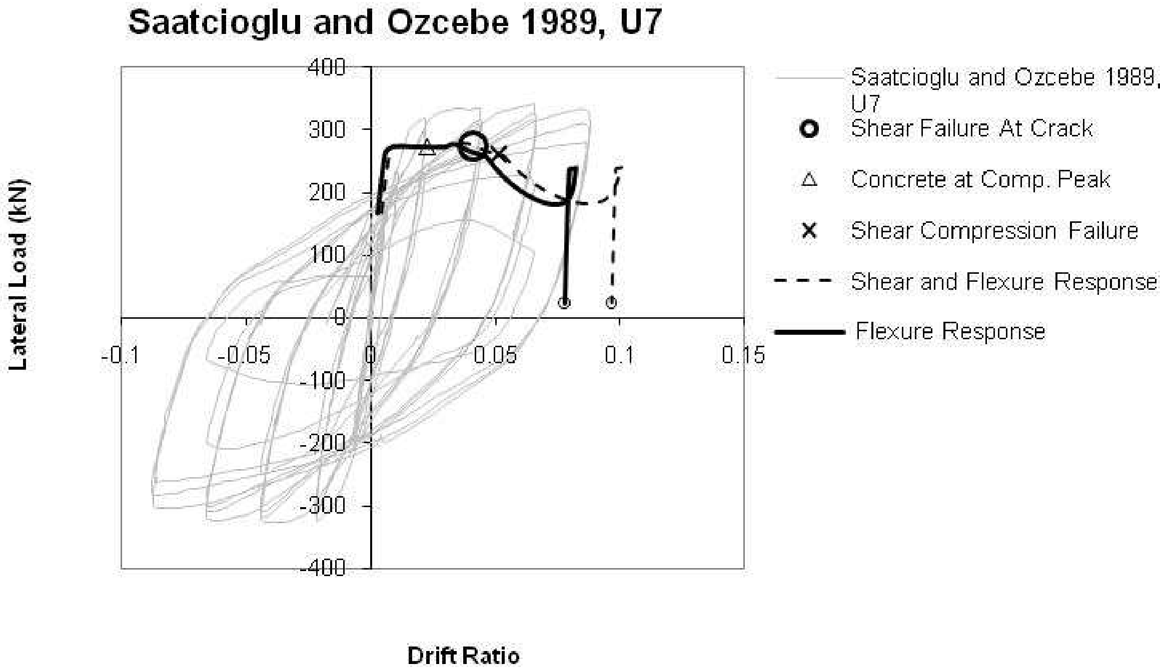

Figure 45. Saatcioglu and Ozcebe 1989, U7.

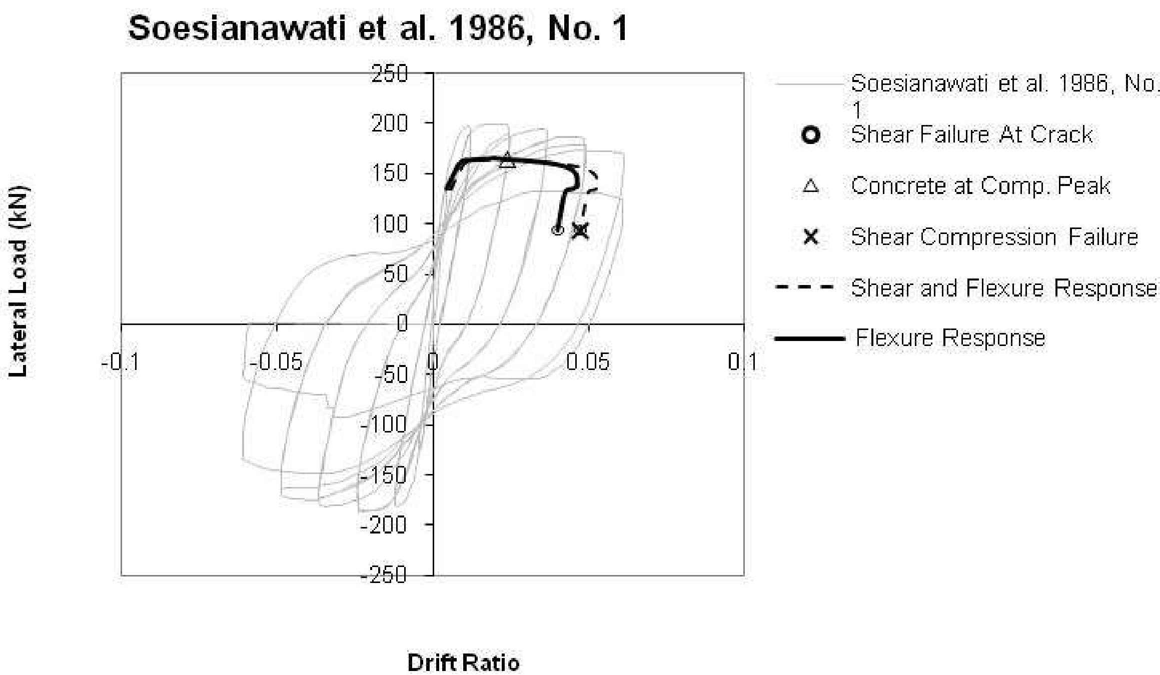

Figure 46. Soesianawati et al. 1986, No. 1.

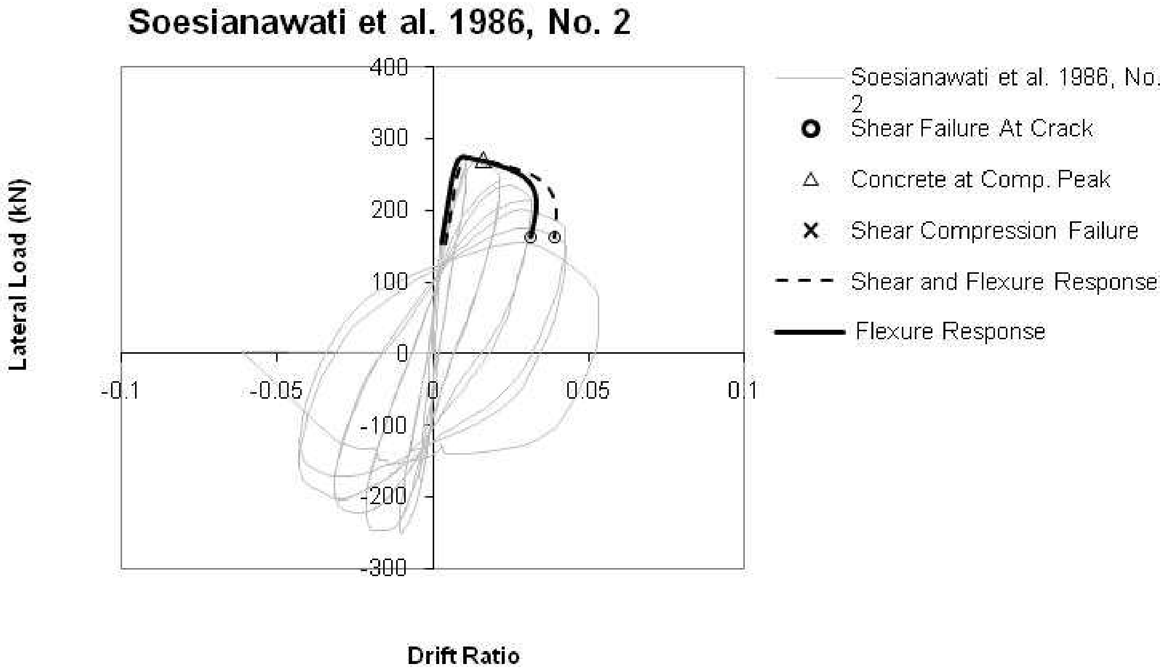

Figure 47. Soesianawati et al. 1986, No. 2.

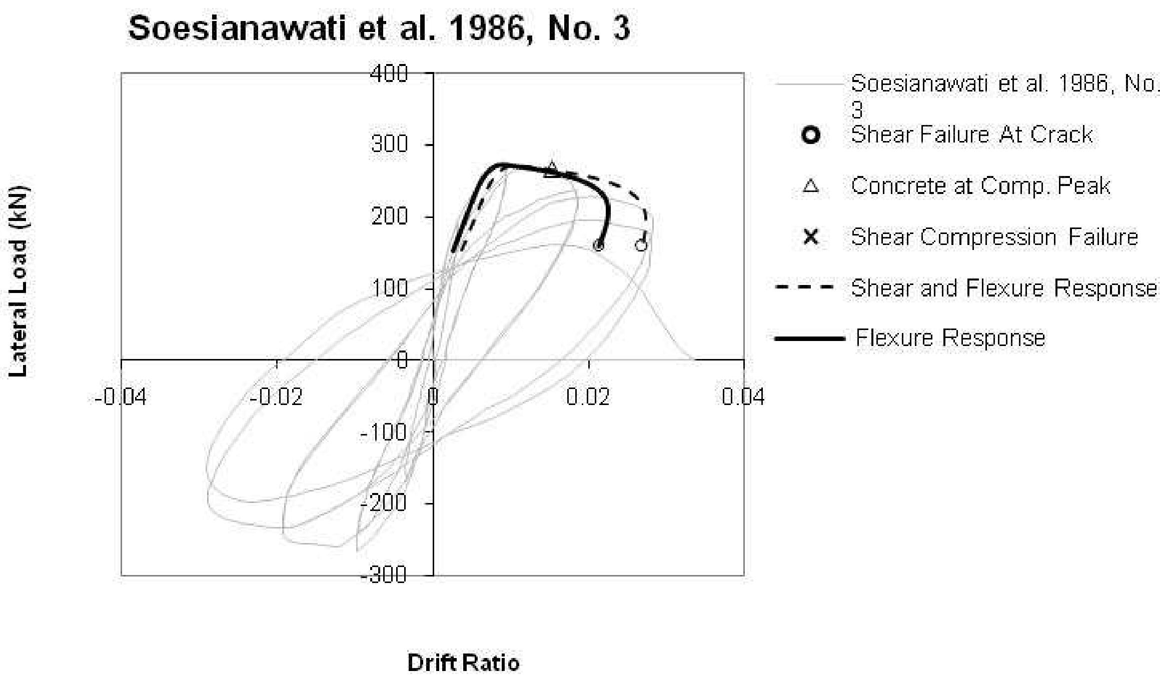

Figure 48. Soesianawati et al. 1986, No. 3.

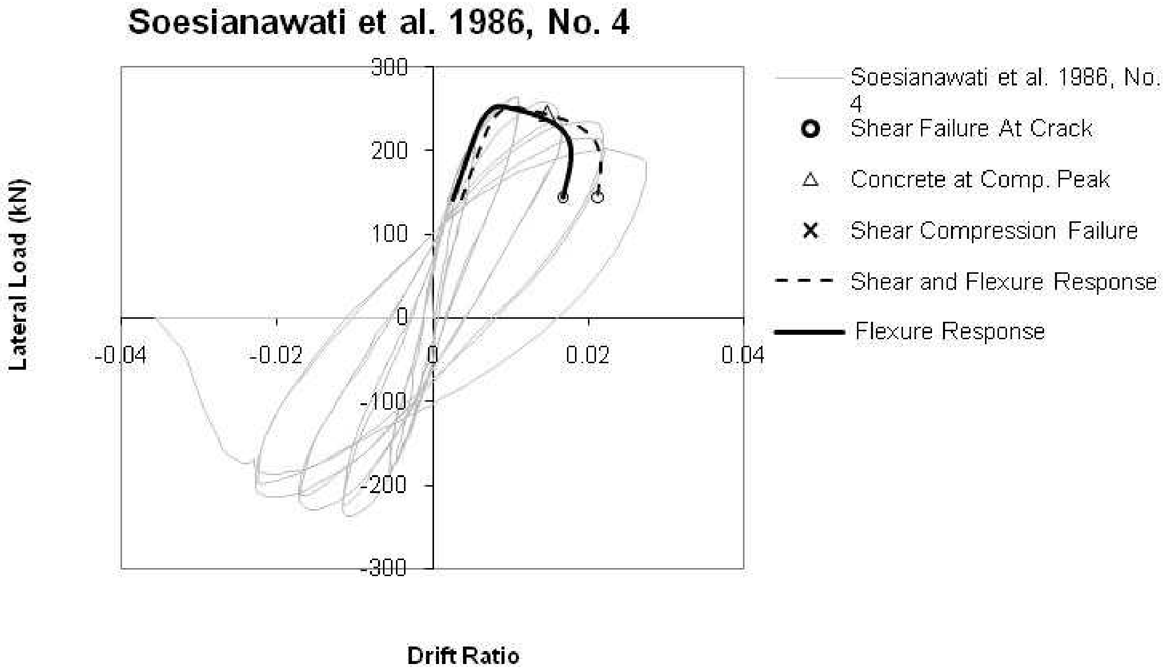

Figure 49. Soesianawati et al. 1986, No. 4.

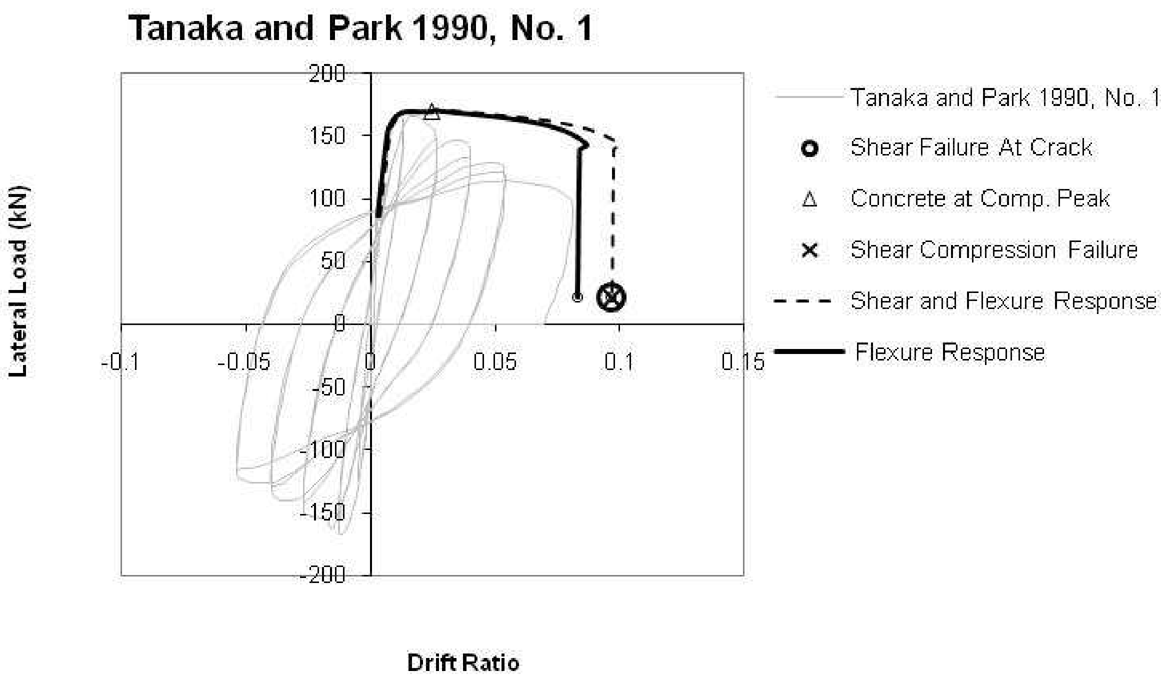

Figure 50. Tanaka and Park 1990, No. 1.

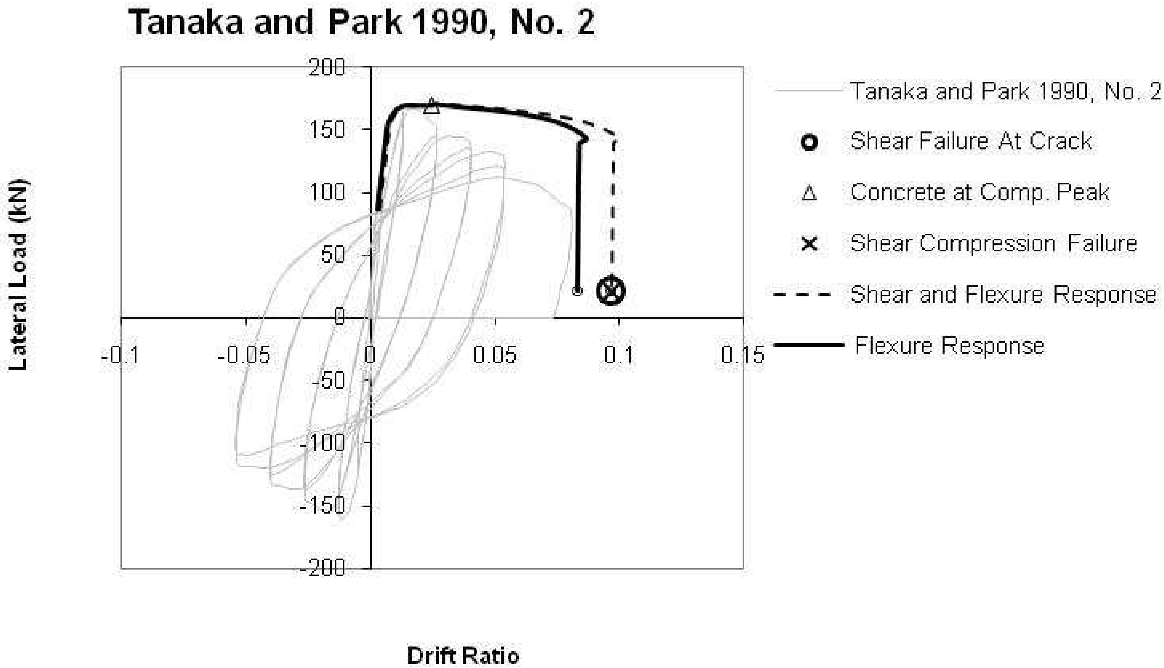

Figure 51. Tanaka and Park 1990, No. 2.

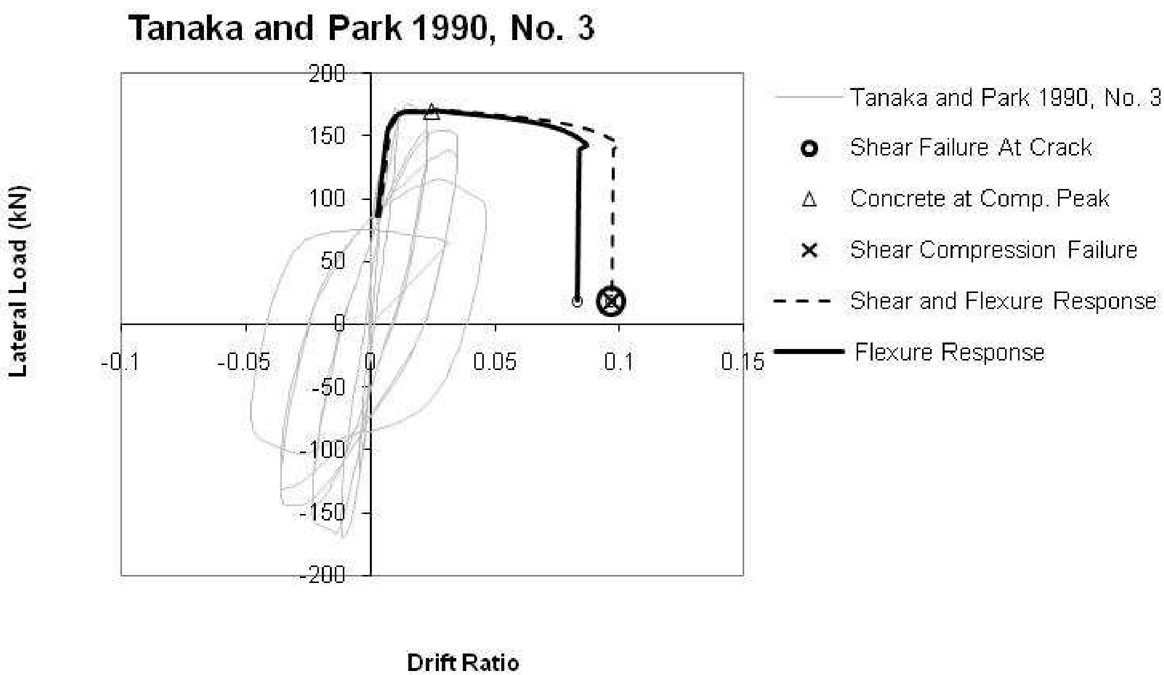

Figure 52. Tanaka and Park 1990, No. 3.

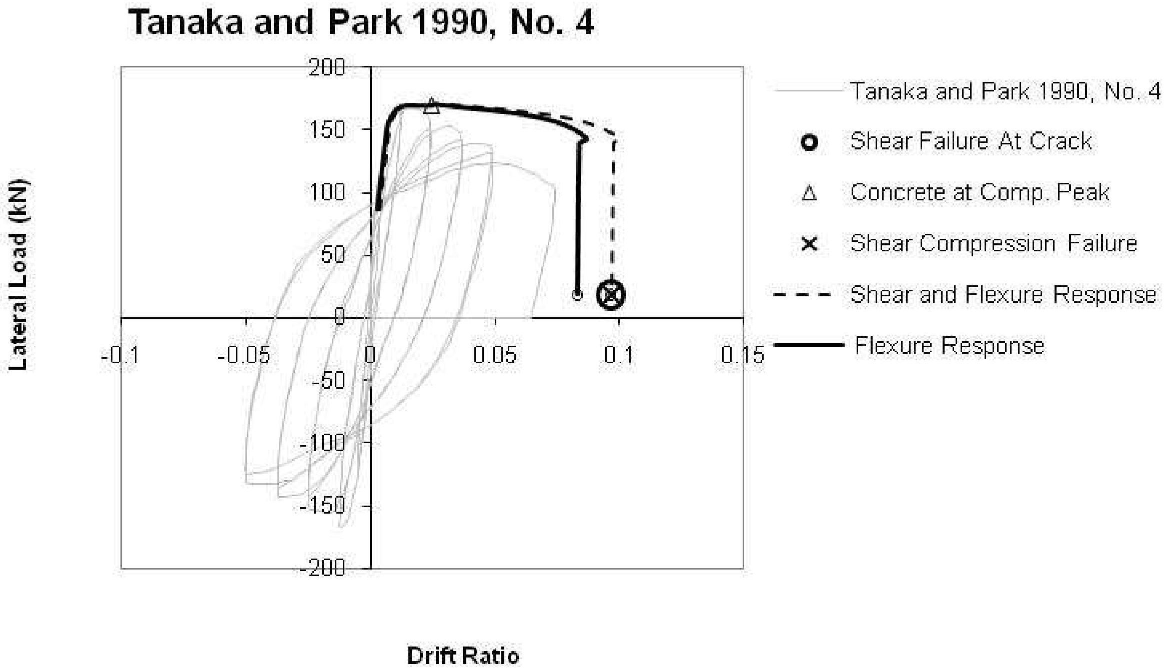

Figure 53. Tanaka and Park 1990, No. 4.

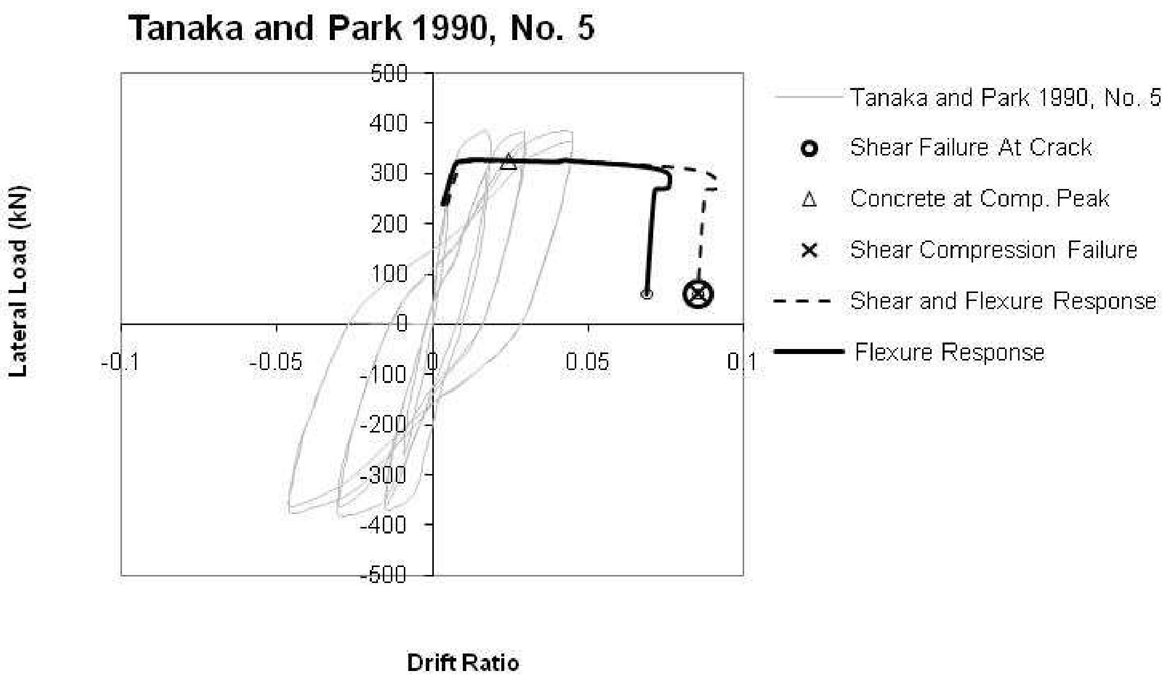

Figure 54. Tanaka and Park 1990, No. 5.

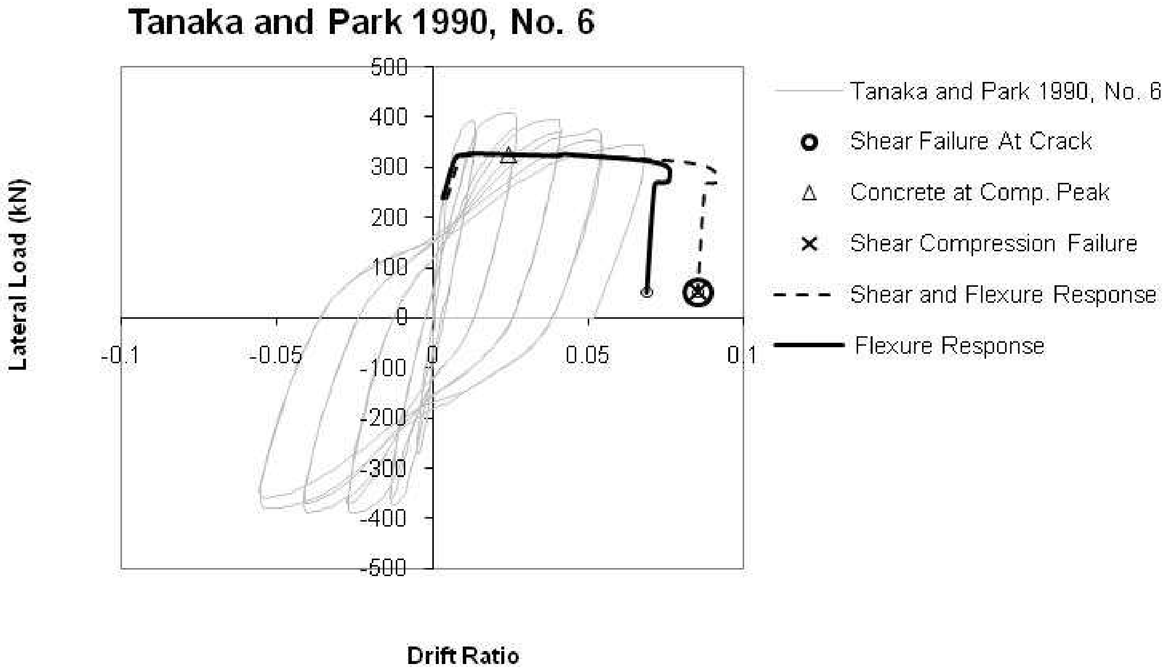

Figure 57. Tanaka and Park 1990, No. 6.

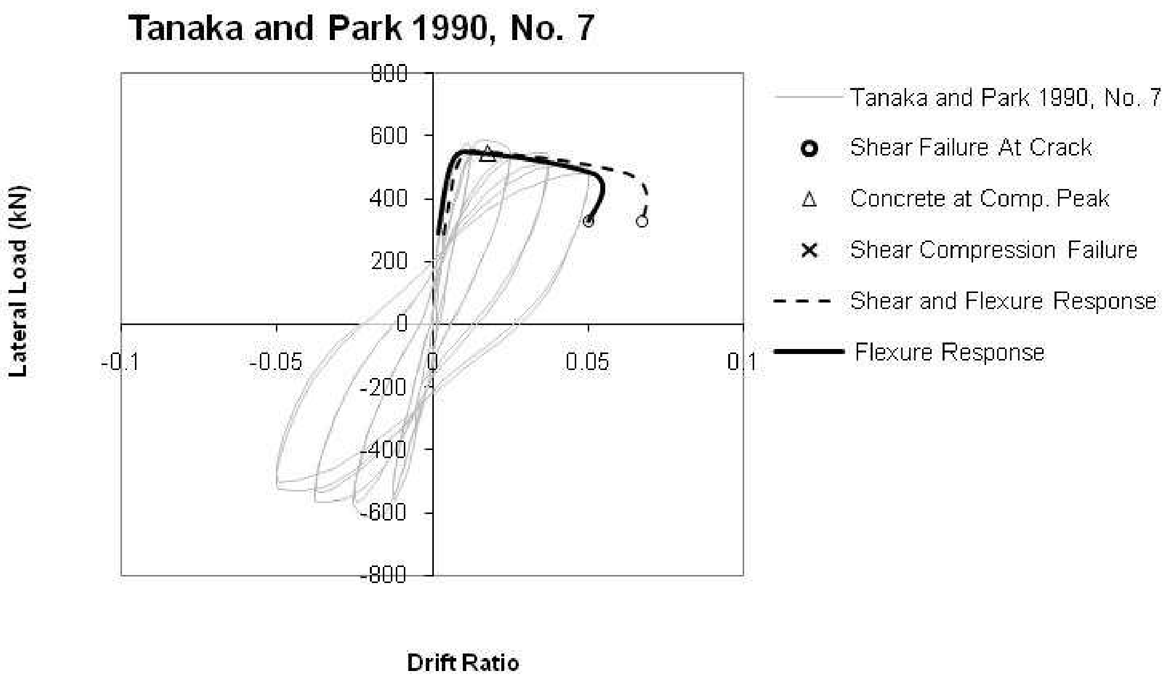

Figure 56. Tanaka and Park 1990, No. 7.

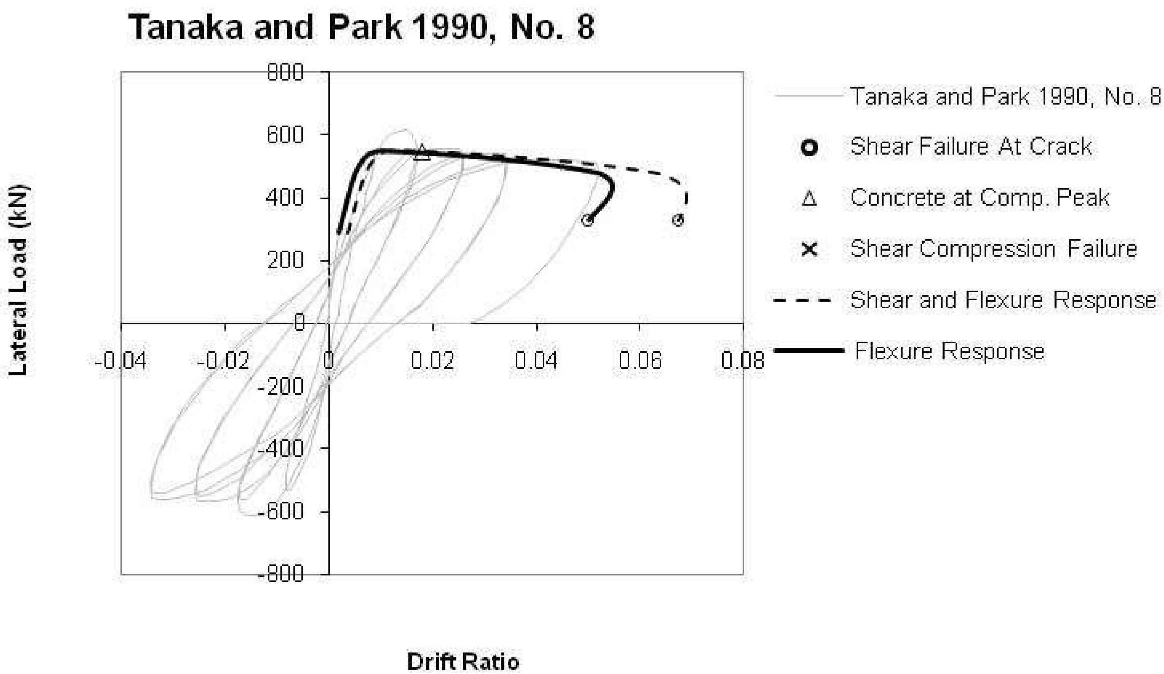

Figure 57. Tanaka and Park 1990, No. 8.

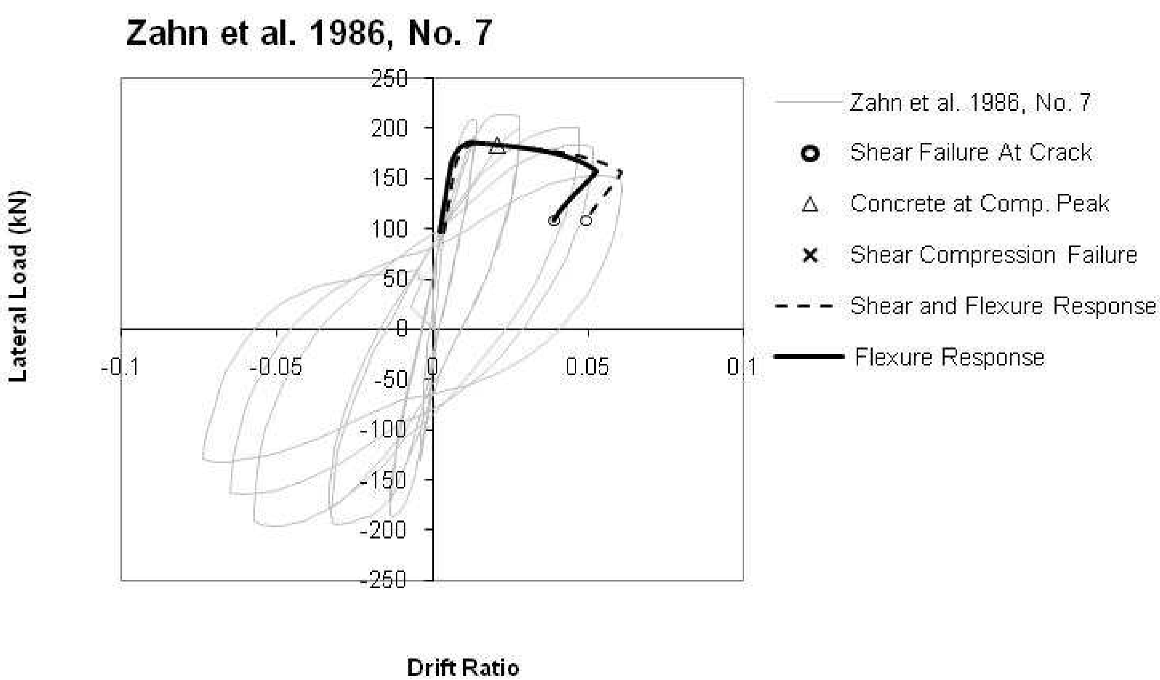

Figure 58. Zahn et al. 1986, No. 7.

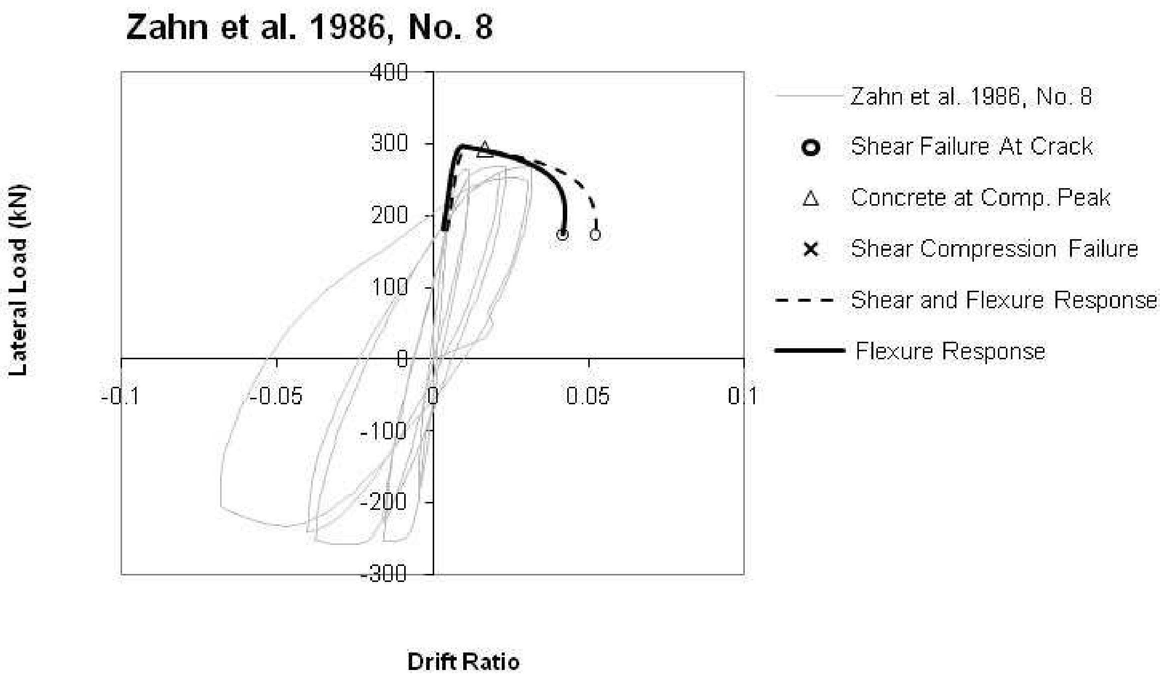

Figure 59. Zahn et al. 1986, No. 8